



Cnidome and Morphological Features of *Pelagia noctiluca* (Cnidaria: Scyphozoa) Throughout the Different Life Cycle Stages

Ainara Ballesteros^{1*}, Carina Östman², Andreu Santín¹, Macarena Marambio¹, Mridvika Narda³ and Josep-Maria Gili¹

¹ Department of Marine Biology and Oceanography, Institute of Marine Sciences (ICM-CSIC), Barcelona, Spain,

² Evolutionary Biology Centre (EBC), Department of Organismal Biology, Uppsala University, Uppsala, Sweden, ³ ISDIN, Innovation and Development, Barcelona, Spain

OPEN ACCESS

Edited by:

Rachel Collin,
Smithsonian Tropical Research
Institute (STI), United States

Reviewed by:

Andre Carrara Morandini,
University of São Paulo, Brazil
Cheryl L. Ames,
Tohoku University, Japan
Maria Pia Miglietta,
Texas A&M University at Galveston,
United States
Massimo Avian,
University of Trieste, Italy

*Correspondence:

Ainara Ballesteros
ballesteros@icm.csic.es

Specialty section:

This article was submitted to
Marine Biology,
a section of the journal
Frontiers in Marine Science

Received: 25 May 2021

Accepted: 13 July 2021

Published: 04 August 2021

Citation:

Ballesteros A, Östman C,
Santín A, Marambio M, Narda M and
Gili J-M (2021) Cnidome
and Morphological Features
of *Pelagia noctiluca* (Cnidaria:
Scyphozoa) Throughout the Different
Life Cycle Stages.
Front. Mar. Sci. 8:714503.
doi: 10.3389/fmars.2021.714503

Pelagia noctiluca is considered the most important jellyfish in the Mediterranean Sea, due to its abundance and the severity of its stings. Despite its importance in marine ecosystems and the health problems caused by its massive arrival in coastal areas, little is known about its early life stages and its cnidome has never been described. This study of the morphological and anatomical features throughout the life cycle identifies four early stages: two ephyra and two metaephyra stages. Ephyra stage 1, newly developed from a planula, has no velar canals, gastric filaments or nematocyst batteries. Ephyra stage 2, has velar canals, a cruciform-shaped manubrium and gastric filaments. Metaephyra stage 3 has eight tentacle buds and nematocyst clusters for the first time. Lastly, in metaephyra stage 4, the eight primary tentacles grow nearly simultaneously, with no secondary tentacles. Complete nematocyst battery patterns gradually develop throughout the later life stages. Four nematocyst types are identified: a-isorhiza, A-isorhiza, O-isorhiza and eurytele. Of these, a-isorhiza and eurytele are the most important throughout the entire life cycle, while A-isorhiza and O-isorhiza have a more important role in advanced stages. All nematocysts show a positive correlation between increasing capsule volumes and increasing body diameter of the ephyrae, metaephyrae, young medusae and adult medusae. In the early stages, the volumes of euryteles in the gastric filaments are larger than those in the exumbrella, indicating that the capsule volume is critical in the absence of marginal tentacles, specialized for feeding. This study provides updated information, the most extensive description to date, including high-resolution photographs and schematic drawings of all the developmental stages in the life cycle of *P. noctiluca*. Additionally, the first cnidome characterization is provided for each stage to facilitate accurate identification of this species when collected in the water column, and to raise awareness of the potential for human envenomation.

Keywords: cnidome, early stage, life cycle, morphology, nematocyst, *Pelagia noctiluca*

Abbreviations: CDD, central disk diameter; CL, capsule length; CV, capsule volume; CW, capsule width; LM, light microscope; LStL, lappet stem length; ML, manubrium length; RA, relative abundance; RLL, rhopalial lappet length; SEM, scanning electron microscope; TBD, total body diameter; TMLL, total marginal lappet length; TMLsL, total marginal lappets length.

INTRODUCTION

The presence of jellyfish blooms has a negative effect on human activities (Purcell et al., 2007) and causes socio-economic and public health problems worldwide (Gili and Pagès, 2005; Purcell et al., 2007; Kingsford et al., 2018). Human activities causing eutrophication, global warming, overfishing and increasing coastal constructions are considered possible significant reasons for jellyfish outbreaks (Purcell et al., 2007; Richardson et al., 2009). Each year, several jellyfish swarms are identified in the Mediterranean Sea (Brotz and Pauly, 2012) and a possible long-term increase of this phenomenon has been reported (Brotz et al., 2012). A first step in the early detection of jellyfish blooms is the identification of the early life stages (Straehler-Pohl and Jarms, 2010; Holst, 2012). Under this premise, an identification system, based on useful keys that describe distinctive morphological features between early stages of scyphozoan species, has been established in the last decade (Straehler-Pohl and Jarms, 2010; Holst, 2012).

Jellyfish stings not only cause discomfort for beach users (Cegolon et al., 2013) but also problems for fishers, who may be stung while taking in fishing nets containing numerous jellyfish (Al-Rubiay et al., 2009). Tourism and fisheries are the industries most affected by jellyfish blooms (Purcell et al., 2007). Though a diversity of jellyfish species exists, like all cnidarians, they share the same fundamental stinging mechanism involving injection of prey and predator with venom-filled stinging cells called cnidocytes (Mariscal, 1974). Cnidocytes contain subcellular capsules called cnidocysts, which can be classified into three main categories: nematocyst, spirocyst and ptychocyst (Mariscal, 1974; Watson and Wood, 1988). The categories of spirocyst and ptychocyst each comprise a specific cnidocyst type, but over thirty different cnidocyst types are classified as nematocysts (Mariscal, 1974), some of which, due to capsule size and shape, tubule length and pattern, including spines, can be differentiated into subtypes (Östman, 2000). Some nematocyst types are considered taxonomically diagnostic, whereas others are common across jellyfish species (Fautin, 2009). The cnidome, the term for the total complement of cnidocytes within a cnidarian specimen (Heins et al., 2015), including their cnidocyst size, abundance and distribution during each developmental life stage, is essential in taxonomic descriptions (Weill, 1934; Calder, 1983; Östman, 2000; Fautin, 2009). The criteria for nematocyst classification have changed with the advent of the scanning electron microscope (SEM) and improved light microscopic (LM) resolution (Shostak and Kolluri, 1995). Advances in microscopic observation techniques have revealed errors in the traditional nomenclature (Östman, 2000), hence the need to re-examine and reclassify some cnidocytes.

Scyphozoan life cycles vary among species from metagenetic to holoplanktonic (Ceh et al., 2015). A metagenetic life cycle implies an alternation between different life forms and reproductive models (Ceh et al., 2015). Fertilized eggs from adult medusae metamorphose to planulae, which attach to benthic substrates, giving rise to an asexually reproducing polyp (benthic life phase) (Fuentes et al., 2011). In optimal environmental conditions (Ceh et al., 2015), perpendicular polyp fission, called

strobilation, gives rise to multiple ephyrae, which will become part of the pelagic life (pelagic life phase). Ephyrae then grow into sexually reproductive medusae, closing the life cycle (Fuentes et al., 2011).

The alternation between sexual and asexual generations does not always occur in scyphozoans (Helm, 2018). Planulae can metamorphose directly to ephyrae, thus lacking the polyp phase. This is the case for *Pelagia noctiluca* (Rottini Sandrini and Avian, 1983; Canepa et al., 2014; Helm et al., 2015; Ramondenc et al., 2019), one of the few scyphozoans with life cycle variations (Helm, 2018) and the only species within the Pelagiidae family (Helm et al., 2015). The holoplanktonic life cycle of *P. noctiluca* is an important difference from the metagenetic life cycle of other common Mediterranean jellyfish such as *Cotylorhiza tuberculata*, *Rhizostoma pulmo*, and *Aurelia aurita* (Kikinger, 1992; Fuentes et al., 2011; Matveev et al., 2012). Therefore, studying their holoplanktonic life cycle provides a unique opportunity to understand the evolutionary simplification and its developmental implications (Helm et al., 2015).

The mauve stinger, *P. noctiluca*, is recognized as the most important jellyfish in the Mediterranean Sea (Brotz and Pauly, 2012; Canepa et al., 2014) due to its abundance along the basin and the severity of its sting (Mariottini et al., 2008; Marambio et al., 2021b). Generally, the sting produces local symptoms such as severe pain, burning sensation, erythema, edema and vesicles (Cegolon et al., 2013; Montgomery et al., 2016; Hall, 2018). As systemic symptoms are uncommon, *P. noctiluca* is considered a non-life-threatening species (Cegolon et al., 2013). Owing to the high number of stings seen by lifeguard services (De Donno et al., 2014), the efforts of the scientific community are focused on sting prevention and management of the mauve stinger (Morabito et al., 2014, 2020; Hall, 2018; Ballesteros et al., 2021).

The life cycle of *P. noctiluca* was described in the monograph 'Medusae of the British Isles' (Russell, 1970). The simple, schematic drawings, especially of the early developmental stages, are difficult to compare with living or preserved individuals in plankton samples (Holst, 2012). Despite the notoriety of *P. noctiluca* in the Mediterranean Sea (Brotz and Pauly, 2012; Canepa et al., 2014) and elsewhere (Mariottini et al., 2008), this species has not been included in the current reference studies for identification of early planktonic scyphozoan stages (Straehler-Pohl and Jarms, 2010; Straehler-Pohl et al., 2011; Holst, 2012).

Pelagia noctiluca is a non-selective predator (Milisenda et al., 2018). Its nematocysts capture a wide variety of prey, copepods being one of the main items (Sabatés et al., 2010; Tilves et al., 2016). While the nematocysts types of adult *P. noctiluca* were previously identified (Krasinska, 1914; Weill, 1934; Quadrifoglio et al., 1986; Larson, 1987; Avian et al., 1991; Marchini et al., 2004; Sánchez-Rodríguez and Lucio-Martínez, 2011), the complete and detailed cnidome for the entire life cycle has never been described.

To provide morphological information on the early life stages and cnidome of *P. noctiluca*, the goals of our study were to: (I) re-examine and classify the nematocysts, applying current nematocyst classifications, (II) describe the developmental stages during the life cycle, including the cnidome as an important taxonomic characteristic and (III) analyze the nematocyst capsule

volumes in relation to body diameter during the different development stages.

MATERIALS AND METHODS

Culture and Growth of *Pelagia noctiluca*

Twelve randomly selected, sexually mature jellyfish were collected in April 2019 on the Catalan coast (Port de la Selva, Spain) during a *P. noctiluca* bloom, using hand nets and plastic jars. The individuals were then transferred to plastic bags full of seawater, avoiding air bubbles to ensure good conditions during transport. The jellyfish were relocated in a kreisel tank (400L capacity, 37–38‰ salinity, 21°C temperature and light cycle of 12 h light/12 h dark) in the Aquarium Experimental Zone (ZAE) at the Institute of Marine Sciences in Barcelona, Spain.

The next morning, mucus strips with fertilized eggs were transferred using a wide plastic pipette to a plastic jug with natural filtered seawater (37–38‰ salinity) and abundant aeration. The plastic jug was situated in a culture room (18°C temperature and light cycle of 12 h light/12 h dark). Within 4 days, eggs metamorphosed into planula larvae and later, ephyrae were observed.

Early life cycle stages (ephyra and metaephyra) were cultured in plastic jugs with aeration; cultures were placed in the culture room with the conditions as described above and a complete cleaning every 3 days, involving removal of individuals one by one with a plastic pipette and complete replacement of seawater.

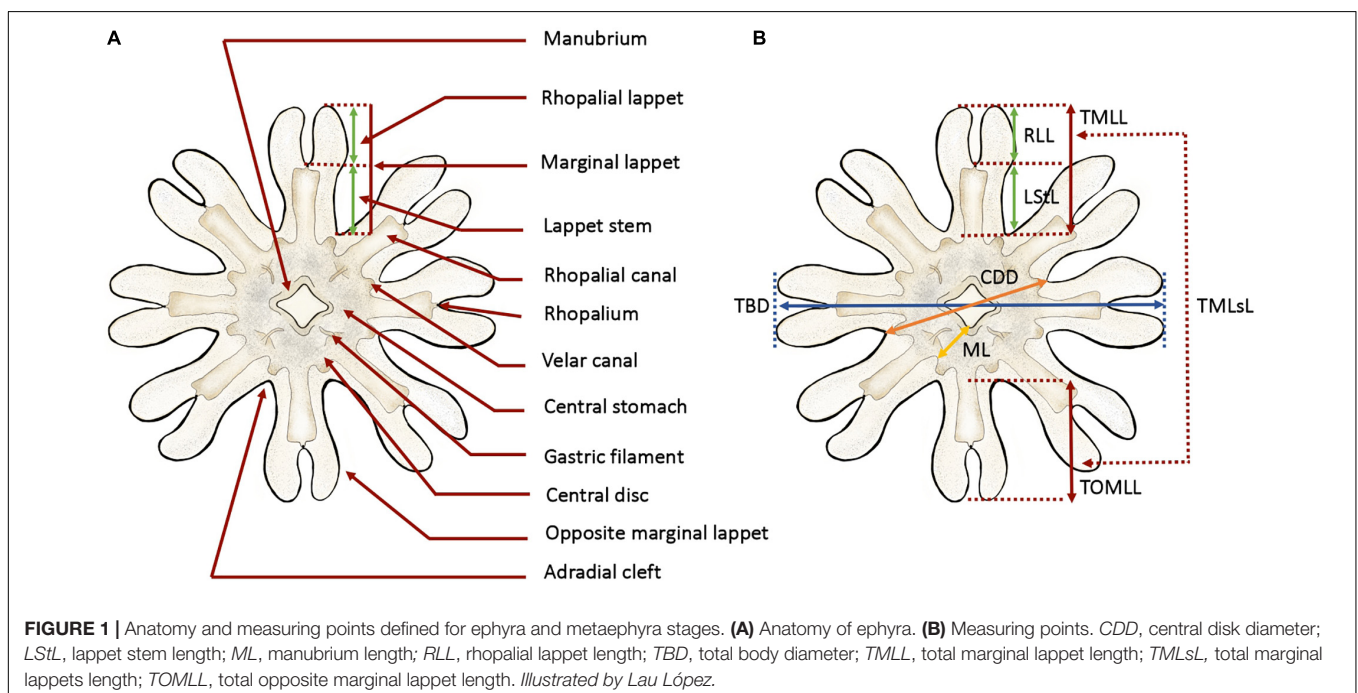
For the juvenile and adult medusa stages, open seawater circulation in kreisel tanks was selected. The kreisel tank capacities were 50L for young juveniles and 400L for the most developed juveniles and adult medusae (37–38‰ salinity, 21°C temperature and light cycle of 12 h light/12 h dark).

Individuals were fed daily, with a varied diet according to the different life cycle stages. Ephyrae and metaephyrae were fed with *Brachiouonus* sp. cultures, newly hatched *Artemia* sp., chopped nauplii and *Aurelia* sp. mucus. Young medusae were fed with *Artemia* sp. nauplii and small pieces of the jellyfish *Aurelia* sp. For the most developed juveniles and adult medusae, eggs of *Merluccius merluccius*, *Parapenaeus longirostris* and pieces of the jellyfish *Cassiopea* sp. were added to the diet.

Life Cycle Description

The morphological description was mainly focused on the early development stages (ephyrae and metaephyrae). On a weekly basis, 15 living individuals were collected from the culture aquarium for analysis. Individuals were relaxed with a menthol solution (4% w/v) transferred with the manubrium positioned upward (ventral view) to a glass slide and photographed using a binocular loupe (Leica M205 C). The smallest ephyrae were analyzed under a light microscope (ZEISS Axioskop 2 plus) to obtain more accurate images. Afterward, the individuals were carefully returned to the culture.

To describe the early *P. noctiluca* stages, terminology (Figure 1A) and measuring points (Figure 1B) were defined for scyphozoan ephyrae as in Straehler-Pohl and Jarms (2010) and Straehler-Pohl et al. (2011). The total body diameter (TBD), central disk diameter (CDD), total marginal lappet length (TMLL), lappet stem length (LStL), rhopalial lappet length (RLL) and manubrium length (ML) were measured. In addition, we calculated the total marginal lappets length (TMLsL), where *s* stands for the sum of the total marginal lappet length (TMLL) and the total opposite marginal lappet length (TOMLL) (Figure 1B). Data measurements were obtained by photo analysis with the Fiji version of ImageJ software. A total of 30 ephyrae and 30 metaephyrae were measured.



To compare relative body dimensions during the early developmental stages, the following ratios (%) were calculated from measurement data: $RLL/TBD \times 100$, $LStL/TBD \times 100$, $CDD/TBD \times 100$, $RLL/TMLL \times 100$, $LStL/TML \times 100$, $TMLsL/TBD \times 100$ and $ML/CDD \times 100$.

Morphological changes in juvenile and adult medusae, with a TBD larger than 14.00 mm, were observed directly from the culture. For detailed analysis, the jellyfish were transferred to a plastic tray with a small amount of seawater. TBD was measured with a digital caliper. The individuals were carefully returned to the culture.

Cnidome Analysis

To describe the cnidome of the early life cycle stages and the juvenile and adult *P. noctiluca* medusae, we analyzed nematocyst distribution, abundance and capsule measurements. The individuals were not fed overnight. Cnidome observations were routinely carried out during the early morning hours. Living ephyrae and metaephyrae were transferred to a glass slide and covered with a coverslip. Preparations were examined and photographed with a camera attached to a light microscope (ZEISS Axioskop 2 plus). In jellyfish with TBD larger than 14.00 mm, tissues of the body parts exumbrella, manubrium (oral arms) and marginal tentacles were analyzed. The TBD was calculated as shown in the morphological description (Figure 1B).

Nematocysts were identified according to Weill's (1934) classification system with modifications by Mariscal (1974), Calder (1974), Östman and Hydman (1997), and Östman (2000). The nematocyst nomenclature used was that proposed by Watson and Wood (1988). Undischarged capsules were measured by photo analysis using the Fiji version of ImageJ software. Capsule measurements were taken for capsule length (CL), capsule width (CW) and capsule volume (CV). As described by Östman and Hydman (1997), the protruding apical capsular tip was included in the capsule length measurements (Figure 2A, yellow arrow). Only capsules in a horizontal position showing the protruding apical capsular tip were measured. The nematocyst size was calculated from CV as in Purcell and Mills (1988):

$$CV = \frac{4}{3} \pi ab^2$$

where a is the radius of capsule length and b is the radius of capsule width.

In total, 3440 nematocysts (1389 a-isorhizas, 318 A-isorhizas, 246 O-isorhizas and 1487 euryteles) from 24 individuals in different life cycle stages were examined.

To study the development of nematocyst batteries during the life cycle, the relative abundance (RA) of different nematocyst types in the batteries was analyzed in the exumbrella, manubrium (oral arms) and marginal tentacles. RA was calculated as:

$$RA = \frac{NNT}{NTN} 100$$

where NNT is the total number of nematocysts of a single type and NTN is the total number of nematocysts in the battery.

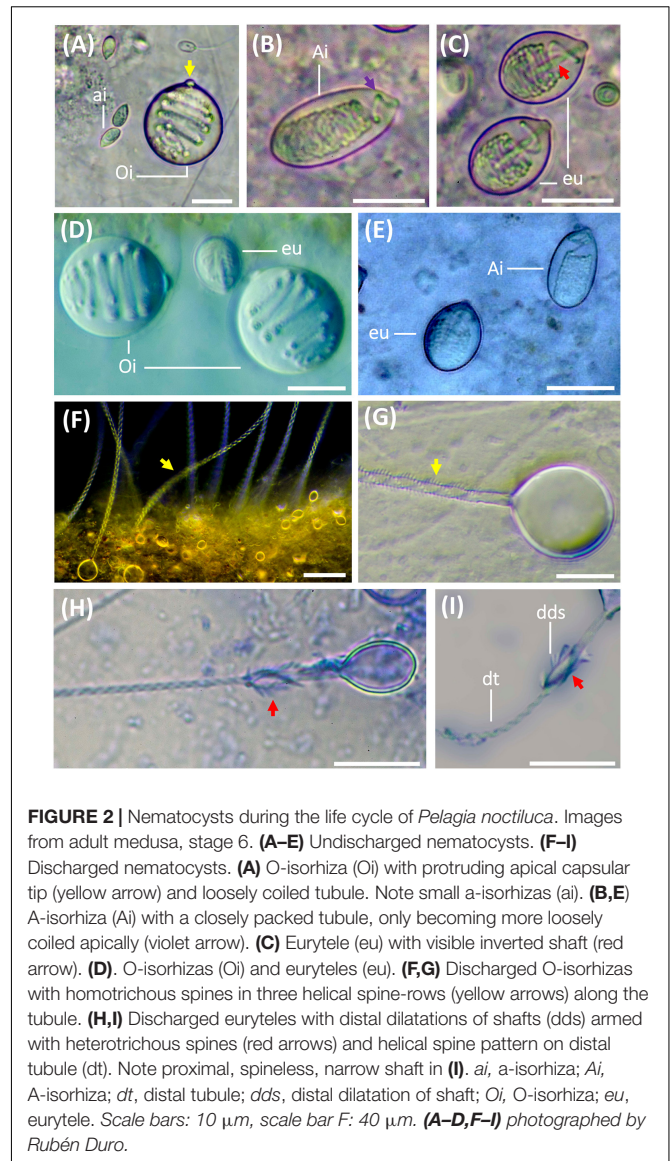


FIGURE 2 | Nematocysts during the life cycle of *Pelagia noctiluca*. Images from adult medusa, stage 6. **(A–E)** Undischarged nematocysts. **(F–I)** Discharged nematocysts. **(A)** O-isorhiza (Oi) with protruding apical capsular tip (yellow arrow) and loosely coiled tubule. Note small a-isorhizas (ai). **(B, E)** A-isorhiza (Ai) with a closely packed tubule, only becoming more loosely coiled apically (violet arrow). **(C)** Eurytele (eu) with visible inverted shaft (red arrow). **(D)** O-isorhizas (Oi) and euryteles (eu). **(F, G)** Discharged O-isorhizas with homotrichous spines in three helical spine-rows (yellow arrows) along the tubule. **(H, I)** Discharged euryteles with distal dilations of shafts (dds) armed with heterotrichous spines (red arrows) and helical spine pattern on distal tubule (dt). Note proximal, spineless, narrow shaft in **(I)**. ai, a-isorhiza; Ai, A-isorhiza; dt, distal tubule; dds, distal dilatation of shaft; Oi, O-isorhiza; eu, eurytele. Scale bars: 10 μm , scale bar F: 40 μm . **(A–D, F–I)** photographed by Rubén Duro.

Statistical Analyses and Graphs

For a more detailed assessment of the possible differences observed in the cnidome composition between body parts along the life cycle of *P. noctiluca*, CV values were grouped by life cycle stage (as defined in Section “Morphology and Cnidome Descriptions”) and tested for statistical differences between groups. All data was first tested for normality and homogeneity using the *shapiro.test* and *barlett.test* functions available as part of the basic stats package from the R software platform (R Core Team, 2017). An ANOVA test was performed using the *aov* function of the *stats* package to test for possible differences in CV in each nematocyst type between: (I) body parts and life cycle stages, (II) body parts within the same life cycle stage and (III) life cycle stages (without considering body parts). To determine between which groups those differences occurred, *post-hoc* analyses were performed using the *pairwise.t.test* function of the *stats* package.

Boxplots were produced to graphically represent differences in CV between nematocyst types and body parts during the different life cycle stages of *P. noctiluca*.

To represent the relative abundance of different nematocyst types in batteries, data were presented in bar graphs for each analyzed body part during the life cycle stages.

Finally, to show the differences in CV throughout the *P. noctiluca* life cycle for each nematocyst type, data were represented using scatterplots for each nematocyst type according to their development stage. Regression lines were added.

RESULTS

Nematocyst Identification

The cnidome of *P. noctiluca* included four different nematocyst types (Figures 2A–C). Three types of homotrichous isorhiza (haplonemes) (Figures 2A,B,F,G) were identified based on the isodiametric tubule, armed with spines of similar size and shape, and lack of well-defined shaft tubule. The fourth nematocyst type was classified as a heterotrichous microbasic eurytele (heteroneme), based on the shaft (shorter than 1.5 times the capsule length) with a clear enlargement of the basal tubule (Figure 2C, red arrow), and a distal dilation armed with prominent spines of different sizes and shapes, in contrast to the smaller spines on the tubule (Figures 2H,I, red arrows).

Other differentiating nematocyst features, such as the capsule volume and shape, pattern of inverted, coiled tubule, and spine pattern on everted tubule and shaft (Figures 2A,B,G), separate a-isorhiza, A-isorhiza and O-isorhiza from each other and from the eurytele. The small a-isorhiza has an oval capsule with regular, horizontally, closely packed tubule coils, except for a few separate coils near the operculum (Figure 2A). The A-isorhiza capsule is large and oval with the tubule closely packed in irregular coils, except apically where it is coiled loosely (Figure 2B, violet arrow). The O-isorhiza capsule is sub-spherical with the broad tubule in regular coils at a right angle to the capsule axis (Figures 2A,D). The discharged O-isorhiza shows three helical rows of homotrichous spines on the isodiametric tubule (Figures 2F,G, yellow arrows). The lemon-shaped eurytele capsule has an inverted rod-shaped shaft (Figure 2C, red arrow), surrounded by regular tubule coils. The discharged eurytele has a differentiated spineless shaft in the proximal part, narrower than the distal shaft dilatation armed with prominent spines (Figures 2H,I, red arrows). The narrow tubule is armed with small spines.

Morphology and Cnidome Descriptions

Planula Larva Stage

Stage 1: The larvae are cone-shaped with a cruciform manubrium. Only a-isorhizas, scattered in great quantities throughout the ectoderm, are identified.

Ephyra Stages

Ephyrae (Figures 3A–D) present octoradial bell symmetry, formed by eight marginal lappets separated by U-shaped adradial

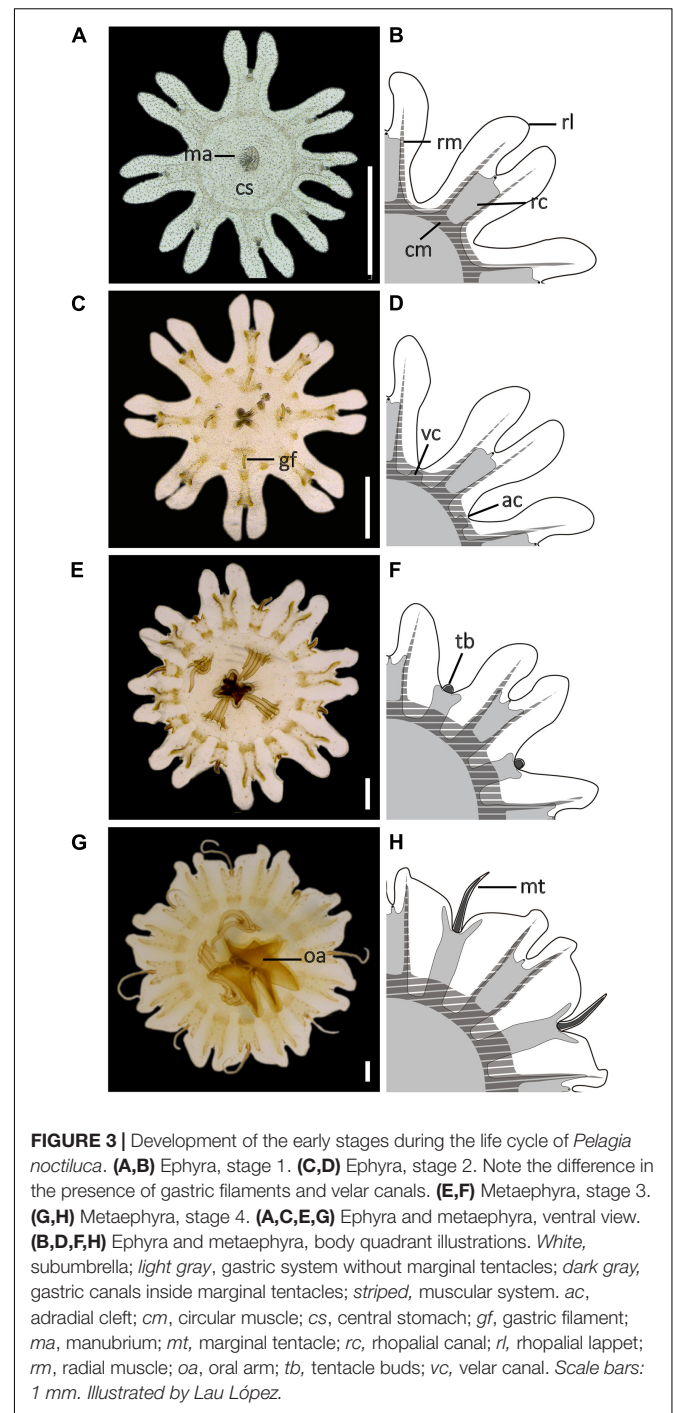


FIGURE 3 | Development of the early stages during the life cycle of *Pelagia noctiluca*. (A,B) Ephyra, stage 1. (C,D) Ephyra, stage 2. Note the difference in the presence of gastric filaments and velar canals. (E,F) Metaephyra, stage 3. (G,H) Metaephyra, stage 4. (A,C,E,G) Ephyra and metaephyra, ventral view. (B,D,F,H) Ephyra and metaephyra, body quadrant illustrations. *White*, subumbrella; *light gray*, gastric system without marginal tentacles; *dark gray*, gastric canals inside marginal tentacles; *striped*, muscular system. *ac*, adradial cleft; *cm*, circular muscle; *cs*, central stomach; *gf*, gastric filament; *ma*, manubrium; *mt*, marginal tentacle; *rc*, rhopalial canal; *rl*, rhopalial lappet; *rm*, radial muscle; *oa*, oral arm; *tb*, tentacle buds; *vc*, velar canal. Scale bars: 1 mm. Illustrated by Lau López.

clefts (Figure 1A). Each marginal lappet is forked distally into a pair of rhopalial lappets (Figure 3B). A single rhopalium is present per lappet stem, between the pair of rhopalial lappets inside the sense niche (Figures 4A,B). A statocyst, composed of reflective crystals, appears at the rhopalium tip (Figure 4B). The ephyrae consist of four morphologically identical quadrants (Figures 3B,D). Two different ephyra stages are identified mainly based on the development of the gastric system including absence or presence of velar canals and gastric filaments (Figures 3A–C).

Stage 1 (Figures 3A,B, 4A–C): Newly developed ephyrae are transparent, with round to oval spoon-shaped rhopalial lappets with rounded tips (Figure 4B). The TBD ranges between 1.80 and 3.00 mm with a mean TBD of ~ 2.50 mm (Table 1). Additional measurements are given in Table 1.

Gastric system

Eight unforked, spade-shaped rhopalial canals (gastric pouches) connect with the central stomach. The terminal rhopalial canal ends at the rhopalium base (Figures 4A,B). Radial muscles, along the rhopalial canals, unite with the weakly developed circular muscle around the central stomach (Figure 3B). In the center of the gastric cavity there is a cruciform-shaped manubrium (Figures 3A, 4C) with no gastric filaments (Figures 3A, 4C).

Cnidome

Single nematocysts are randomly distributed throughout the ephyra (Figure 4B, green arrow). Abundant small a-isorhizas dominate in the exumbrella ectoderm, followed by a few

irregularly distributed euryteles. In the manubrium and nearby areas, a-isorhizas are also present (Table 2). Nematocyst clusters (batteries/warts) are not identified.

Stage 2 (Figures 3C,D, 4D–F): Ephyrae are transparent and brown to ochre-colored, present in areas near the rhopalial canals, velar canals and at the base of the gastric filament quadrants. Rhopalial lappets are oval, spoon-shaped to bread knife-shaped with rounded tips (Figure 4E). The ephyrae grow during the first week reaching between 3.10 and 5.00 mm with a mean TBD of ~ 4.00 mm (Table 1). Additional measurements are given in Table 1.

Gastric system

Eight unforked, spade-shaped velar canals (gastric pouches) are identified (Figures 3D, 4D). Velar canals are connected with each other and with the rhopalial canals and central stomach. Rhopalial canals are unforked and spade-shaped (Figures 4D,E). In each of the four quadrants, 1 to 3 gastric filaments are present above the central stomach (Figures 3C, 4D) with a cruciform-shaped manubrium (Figure 4F).

Cnidome

Abundant small, single a-isorhizas are randomly scattered dominating the exumbrella, followed by some O-isorhizas and euryteles (Figure 4E, green arrows). The manubrium also contains abundant a-isorhizas. Euryteles are the only nematocyst type in the gastric filaments (Table 2).

Metaephyra Stages

Metaephyrae (Figures 3E–H) show some differences from the ephyrae anatomy (Figures 3A–D). Umbrella development causes some significant changes in the body proportions: CDD increases and TMLsL decreases with respect to TBD. The proportion of ML to CDD was closely similar to the ephyra stages, with the manubrium growing proportionally to the growth of the individuals in the early stages. As with ephyrae, the two differentiated metaephyrae are split into 4 identical morphological quadrants (Figures 3E,H).

Stage 3 (Figures 3E,F, 4G–I): Metaephyrae are faint brown to ochre-colored. The terminal end of the velar canal and the base of the rhopalial canals have an intense brownish color, forming a distinct ring above the circular muscle. The manubrium is completely brown. The oval, rhopalial lappets are spoon-shaped to bread knife-shaped with rounded tips (Figure 4H). The TBD ranges between 5.10 and 8.00 mm with a mean TBD of ~ 7.10 mm (Table 1). Additional measurements are given in Table 1.

Gastric system

Rhopalial canals are forked. Fork arms present with rounded tips, growing centrifugally into rhopalial lappets from level with to slightly overstepping the rhopalium tip (Figures 3F, 4G,H). Slightly forked velar canals with rounded tips grow in a centrifugal direction until almost reaching the umbrella rim (U-shaped adradial cleft) (Figures 3F, 4G). Eight tentacle buds or incipient tentacles lie above the velar canals (Figures 3F, 4G). Each body quadrant is formed by 3 to 5 gastric filaments. The manubrium starts to grow longitudinally (Figure 4I).

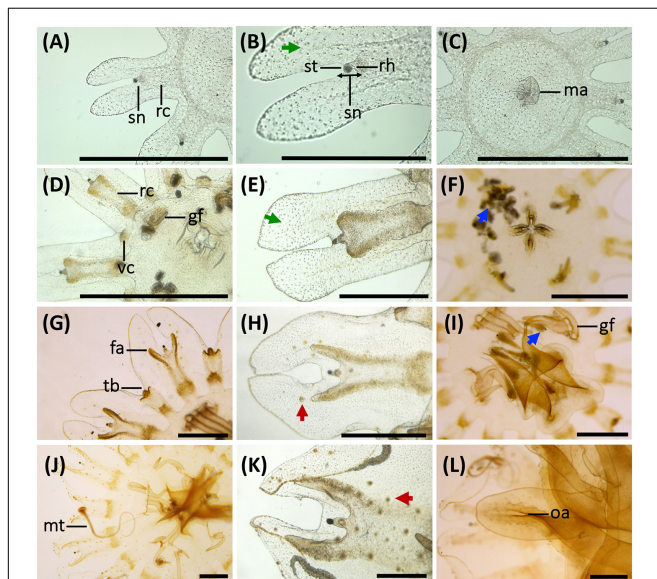
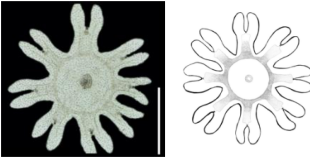
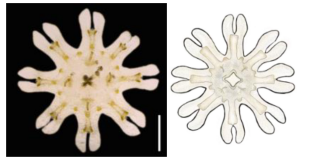
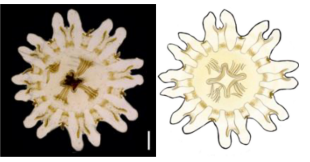



FIGURE 4 | Morphological changes, development of gastric system and cnidae in early stages of the life cycle of *Pelagia noctiluca*. (A–C) Ephyra, stage 1. (D–F) Ephyra, stage 2. (G–I) Metaephyra, stage 3. (J–L) Metaephyra, stage 4. (A,D,G,J) Rhopalial and velar canals. (B,E,H,K) Rhopalial canals and nematocysts in exumbrella. (C,F,I,L) Central disk. (A) Spade-shaped rhopalial canals (rc) and sense niche (sn). (B) Sense niche composed of the rhopalium (rh) and the statocyst (st) at the tip. (C) Central stomach with manubrium (ma). (D) Rhopalial canal (rc) and velar canal (vc). Note initial gastric filaments (gf). (E) Spade-shaped rhopalial canal. (F) *Brachiouinus* sp. (blue arrow) inside the gastric system. (G) Tentacle buds (tb) above velar canals. (G,H) Fork arms (fa) of rhopalium slightly overtop rhopalium. (I) *Artemia* sp. (blue arrow) caught by euryteles in gastric filaments (gf). (J) Marginal tentacles (mt) growing simultaneously. (K) Sharp-shaped rhopalial canals. (L) Initial oral arms (oa). (B,E) Abundant single nematocysts (green arrows). Note absence of nematocyst batteries. (H) First homogenous, round-shaped nematocyst batteries (red arrow). (K) Nematocyst batteries increase in numbers (red arrow), note position close to rhopalial canal. *fa*, fork arm; *gf*, gastric filament; *ma*, manubrium; *mt*, marginal tentacle; *rc*, rhopalial canal; *rh*, rhopalium; *oa*, oral arm; *sc*, statocyst; *sn*, sense niche; *tb*, tentacle bud; *vc*, velar canal. Scale bars: 1 mm, scale bars (B,E): 0.5 mm.

TABLE 1 | Morphology, body proportions and cnidome of the early stages of *Pelagia noctiluca* life cycle.

Ephyra		Metaephyra	
Stage 1	Stage 2	Stage 3	Stage 4
			
TBD range: 1.80–3.00 mm, TBD mean: ~ 2.50 mm	TBD range: 3.10–5.00 mm, TBD mean: ~ 4.00 mm	TBD range: 5.10–8.00 mm, TBD mean: ~ 7.10 mm	TBD range: 8.10–14.00 mm, TBD mean: ~ 11.70 mm
Anatomy: 8 marginal lappets 16 round to oval spoon-like rhopalial lappets, round tips No gastric filaments Long ML, approx. 40% of CDD (SD = 0.03)	Anatomy: 8 marginal lappets 16 oval spoon- to bread knife-shaped rhopalial lappets, round tips 1–3 gastric filaments per quadrant Long ML, approx. 39% of CDD (SD = 0.05)	Anatomy: 8 marginal lappets 16 oval spoon- to bread knife-shaped rhopalial lappets, round tips 3–5 gastric filaments per quadrant Tentacle buds or incipient marginal tentacles Long ML, approx. 37% of CDD (SD = 0.03)	Anatomy: 8 marginal lappets 16 oval spoon- to bread knife-shaped broad rhopalial lappets, round tips 5–8 gastric filaments per quadrant 8 marginal tentacles Long ML, approx. 39% of CDD (SD = 0.04)
Gastric system: Rhopalial canals unforked, spade-shaped No velar canals	Gastric system: Rhopalial canals unforked, spade-shaped Velar canals unforked, spade-shaped	Gastric system: Rhopalial canals forked, round-shaped, fork tips level to slightly overtop rhopalium tip Velar canals slightly forked, round fork tips	Gastric system: Rhopalial canals forked: round to sharp-shaped, fork tips overtop rhopalium Velar canals forked, round fork tips
Mean body proportions: RLL ≈ 14% of TBD (SD = 0.01) LStL ≈ 13% of TBD (SD = 0.01) CDD ≈ 47% of TBD (SD = 0.02) TMLsL ≈ 53% of TBD (SD = 0.02) LStL ≈ 47% of TMLL (SD = 0.03) RLL ≈ 53% of TMLL (SD = 0.03)	Mean body proportions: RLL ≈ 13% of TBD (SD = 0.01) LStL ≈ 13% of TBD (SD = 0.02) CDD ≈ 48% of TBD (SD = 0.03) TMLsL ≈ 52% of TBD (SD = 0.03) LStL ≈ 50% of TMLL (SD = 0.05) RLL ≈ 50% of TMLL (SD = 0.05)	Mean body proportions: RLL ≈ 11% of TBD (SD = 0.01) LStL ≈ 8% of TBD (SD = 0.01) CDD ≈ 64% of TBD (SD = 0.02) TMLsL ≈ 36% of TBD (SD = 0.02) LStL ≈ 42% of TMLL (SD = 0.04) RLL ≈ 58% of TMLL (SD = 0.08)	Mean body proportions: RLL ≈ 9% of TBD (SD = 0.02) LStL ≈ 5% of TBD (SD = 0.01) CDD ≈ 72% of t TBD (SD = 0.04) TMLsL ≈ 28% of TBD (SD = 0.04) LStL ≈ 39% of TMLL (SD = 0.05) RLL ≈ 61% of TMLL (SD = 0.05)
Cnidome: Exumbrella: randomly scattered small a-isorhizas dominate, followed by some euryteles No nematocyst batteries	Cnidome: Exumbrella: randomly scattered small a-isorhizas dominate, followed by some euryteles No nematocyst batteries	Cnidome: Exumbrella: randomly scattered small a-isorhizas dominate, followed by some O-isorhizas and euryteles Small nematocyst batteries	Cnidome: Exumbrella: randomly scattered small a-isorhizas dominate, followed by some O-isorhizas, A-isorhizas and euryteles Nematocyst batteries increase in number

CDD, central disk diameter; LStL, lappet stem length; ML, manubrium length; RLL, rhopalial lappet length; SD, standard deviation; TBD, total body diameter; TMLL, total marginal lappet length; TMLsL, total marginal lappets length. Scale bars: 1 mm. Illustrated by Lau López.

Cnidome

Several homogenous, round-shaped nematocyst batteries appear as protrusions in the exumbrella ectoderm (Figure 4H, red arrow). Among the abundant scattered individual nematocysts, a-isorhizas dominate, followed by O-isorhizas and euryteles (Figure 5A). A strong association is observed between position and size of nematocyst warts and degree of pigmentation, from brown to ochre (Figure 4H). Two parallel rows of nematocyst warts and pigment appears at the base of both rhopalial and velar canals, sometimes reaching the umbrella margin (Figure 4H). Scattered nematocyst clusters are also present around the central stomach. In more developed individuals, a few nematocyst batteries are identified at the incipient manubrium base, while a-isorhizas are abundant and randomly distributed. Euryteles are still the only nematocyst type present in the gastric filaments (Table 2).

Stage 4 (Figures 3G,H, 4J–L): Coloration is similar to the previous stage. Rhopalial lappets are bread knife-shaped (Figure 4K). The TBD ranged between of 8.10 and 14.00 mm with

a mean TBD of ~ 11.70 mm (Table 1). Additional measurements given in Table 1.

Gastric system

Fork arms of rhopalial canals grow further into the rhopalial lappets. Their round to sharp-shaped fork tips overstep the rhopalium tip (Figures 3H, 4K). Velar canals, forked with round-shaped tips, grow in a centrifugal direction into marginal lappets, following the complete umbrella shape (Figure 3H) with widening marginal lappets (Figures 3G,H). Nearly simultaneously, all marginal tentacles grow as extensions to velar canals and parallel to marginal lappets (Figures 3G,H). Each body quadrant has 5 to 8 gastric filaments. The manubrium is divided distally into 4 incipient oral arms (Figure 4L), in which an oral groove and thin oral margin are differentiated (Figure 6D).

Cnidome

Copious, scattered, small a-isorhiza dominate in the exumbrella (Figure 7A, red color). Warts, more obvious than in the previous stage, increase in nematocyst number, size and

TABLE 2 | Nematocyst capsule, abundance and measurements from different body parts in each stage during *Pelagia noctiluca* life cycle.

Stage (number of specimens)	Body parts	Nematocyst type (number)	Abundance	Capsule Length Mean \pm SD (μm)	Capsule Width Mean \pm SD (μm)	Capsule Length \times Width Range (μm)	Capsule Volume Mean \pm SD (μm^3)	Capsule Volume Range (μm^3)	
Planula larva 0 (3)	Whole body	a-isorhiza (–)	++++	–	–	–	–	–	
Ephyra 1 (3)	Exumbrella	a-isorhiza (83)	++++	3.70 \pm 0.39	2.79 \pm 0.31	2.24–4.97 \times 2.11–3.65	15.42 \pm 4.16	7.40–24.87	
		A-isorhiza (–)	absent	–	–	–	–	–	
		O-isorhiza (–)	absent	–	–	–	–	–	
	Manubrium	Eurytele (10)	+	6.38 \pm 0.74	5.22 \pm 0.52	5.12–7.99 \times 4.51–6.10	93.38 \pm 29.33	55.35–155.80	
		a-isorhiza (11)	++	3.66 \pm 0.33	2.70 \pm 0.37	3.16–4.31 \times 2.10–3.24	14.39 \pm 4.69	7.64–20.45	
		A-isorhiza (–)	absent	–	–	–	–	–	
Ephyra 2 (3)	Exumbrella	O-isorhiza (–)	absent	–	–	–	–	–	
		Eurytele (–)	absent	–	–	–	–	–	
		a-isorhiza (93)	++++	4.27 \pm 0.49	2.93 \pm 0.45	3.15–6.02 \times 2.00–4.63	20.09 \pm 8.82	8.26–67.45	
		A-isorhiza (–)	absent	–	–	–	–	–	
		O-isorhiza (3)	rare to +	14.52 \pm 1.43	13.05 \pm 1.40	13.51–15.53 \times 12.06–14.04	1315.87 \pm 405.92	1028.84–1602.40	
		Eurytele (3)	+	9.30 \pm 2.01	6.69 \pm 0.85	8.09–11.62 \times 6.13–7.67	228.42 \pm 112.18	161.34–357.93	
		Manubrium	a-isorhiza (17)	+++	4.35 \pm 0.47	3.36 \pm 0.39	3.37–5.36 \times 2.67–4.23	26.33 \pm 7.10	12.58–37.19
			A-isorhiza (–)	absent	–	–	–	–	–
	O-isorhiza (–)		absent	–	–	–	–	–	
	Gastric filaments	Eurytele (–)	absent	–	–	–	–	–	
		a-isorhiza (–)	absent	–	–	–	–	–	
		A-isorhiza (–)	absent	–	–	–	–	–	
O-isorhiza (–)		absent	–	–	–	–	–		
Metaephyra 3 (3)	Exumbrella	Eurytele (11)	exclusive	14.16 \pm 1.25	10.89 \pm 1.13	12.18–16.24 \times 9.03–12.19	901.77 \pm 251.05	520.02–1243.65	
		a-isorhiza (111)	++++	4.64 \pm 0.38	3.18 \pm 0.33	3.43–5.51 \times 2.55–3.99	25.07 \pm 6.40	12.63–44.27	
		A-isorhiza (–)	absent	–	–	–	–	–	
		O-isorhiza (4)	+	14.31 \pm 0.90	13.10 \pm 0.71	1.05–15.15 \times 12.37–13.79	901.77 \pm 251.05	1089.98–1507.11	
		Eurytele (18)	++	10.66 \pm 1.58	8.17 \pm 1.38	8.11–13.93 \times 5.80–11.08	400.00 \pm 196.21	142.89–894.65	
		Manubrium	a-isorhiza (16)	+++	4.54 \pm 0.46	3.37 \pm 0.44	3.63–5.33 \times 2.12–3.87	28.03 \pm 8.44	8.54–40.51
			A-isorhiza (–)	absent	–	–	–	–	–
	O-isorhiza (–)		absent	–	–	–	–	–	
	Gastric filaments	Eurytele (–)	absent	–	–	–	–	–	
		a-isorhiza (–)	absent	–	–	–	–	–	
A-isorhiza (–)		absent	–	–	–	–	–		
Metaephyra 4 (3)	Exumbrella	O-isorhiza (–)	absent	–	–	–	–	–	
		Eurytele (35)	exclusive	13.92 \pm 1.27	10.35 \pm 0.83	11.06–16.15 \times 8.33–11.50	794.39 \pm 180.07	486.82–1074.87	
		a-isorhiza (58)	++++	4.77 \pm 0.46	3.35 \pm 0.32	3.76–5.88 \times 2.58–4.24	28.45 \pm 6.81	16.74–53.26	
		A-isorhiza (3)	rare to +	10.02 \pm 1.00	6.62 \pm 0.64	8.89–10.76 \times 5.90–7.10	234.25 \pm 62.74	161.98–274.85	
		O-isorhiza (3)	absent to +	13.97 \pm 1.11	13.26 \pm 0.36	13.018–14.75 \times 13.01–13.52	1289.91 \pm 172.06	1168.25–1411.58	
		Eurytele (50)	+++	10.83 \pm 1.23	8.15 \pm 1.00	8.61–14.19 \times 6.18–10.63	391.54 \pm 143.02	172.40–839.77	
		Manubrium	a-isorhiza (17)	++++	4.90 \pm 0.52	3.38 \pm 0.28	3.99–5.64 \times 3.04–3.85	29.54 \pm 6.16	19.94–42.45
	A-isorhiza (6)		absent to +	9.90 \pm 0.47	6.87 \pm 0.56	9.16–10.46 \times 6.21–7.45	246.18 \pm 43.56	196.47–303.98	
	O-isorhiza (5)		absent to +	13.64 \pm 0.80	11.85 \pm 0.90	12.65–14.79 \times 11.09–13.12	1014.04 \pm 212.55	1332.93–5070.18	
		Eurytele (18)	+++	11.46 \pm 0.77	7.73 \pm 0.53	10.46–12.82 \times 6.54–8.86	361.38 \pm 64.65	238.51–478.16	

(Continued)

TABLE 2 | Continued

Stage (number of specimens)	Body parts	Nematocyst type (number)	Abundance	Capsule Length Mean ± SD (μm)	Capsule Width Mean ± SD (μm)	Capsule Length × Width Range (μm)	Capsule Volume Mean ± SD (μm ³)	Capsule Volume Range (μm ³)	
Metaephyra 4 (3)	Gastric filaments	a-isorhiza (–)	absent	–	–	–	–	–	
		A-isorhiza (–)	absent	–	–	–	–	–	
		O-isorhiza (–)	absent	–	–	–	–	–	
		Eurytele (19)	exclusive	13.92 ± 1.27	10.35 ± 0.83	11.06–16.15 × 8.33– 11.50	794.39 ± 180.07	486.82– 1074.87	
	Tentacles	a-isorhiza (33)	++++	4.62 ± 0.71	3.17 ± 0.58	3.44–6.10 × 2.21–4.25	26.22 ± 12.58	8.90–56.89	
		A-isorhiza (–)	absent	–	–	–	–	–	
Juvenile 5 (10)	Exumbrella	a-isorhiza (117)	++++	5.52 ± 0.68	3.45 ± 0.54	4.21–7.57 × 2.16–5.41	37.86 ± 15.38	12.57–105.08	
		A-isorhiza (3)	rare to +	10.61 ± 0.40	6.94 ± 0.21	10.32–10.89 × 6.79– 7.08	266.87 ± 5.64	262.89–270.86	
		O-isorhiza (71)	absent to +	18.55 ± 3.04	16.59 ± 2.56	12.34–25.51 × 11.64– 23.10	2859.55 ± 12883.25	874.99– 7130.14	
		Eurytele (293)	+++	12.72 ± 1.60	9.09 ± 1.32	9.29–15.10 × 5.98– 10.56	579.16 ± 228.41	175.60 1280.17	
	Manubrium	a-isorhiza (230)	++++	6.04 ± 0.88	3.69 ± 0.51	4.43–8.47 × 2.69–6.29	44.87 ± 17.19	16.78–131.55	
		A-isorhiza (33)	absent to +	11.66 ± 1.43	7.37 ± 0.86	9.25–13.75 × 5.29– 8.80	339.90 ± 94.16	150.48–499.95 65632–	
		O-isorhiza (60)	absent to ++	16.51 ± 2.39	14.86 ± 2.32	12.11–21.76 × 10.16– 20.14	2036.07 ± 920.02	4621.37	
		Eurytele (284)	+++	11.82 ± 1.03	8.35 ± 0.78	9.50–15.10 × 5.98– 10.56	440.21 ± 111.59	198.48–806.66	
	Tentacles	a-isorhiza (383)	++++	5.69 ± 0.75	3.63 ± 0.54	3.85–8.33 × 2.10–5.82	41.20 ± 17.05	11.95–120.77	
		A-isorhiza (207)	absent to ++	12.37 ± 0.91	7.36 ± 0.79	10.21–14.49 × 4.94– 9.29	357.48 ± 92.41	161.77–652.44	
		O-isorhiza (1)	absent to +	17.46	15.81	17.46–15.81	2285.11	–	
	Adult 6 (2)	Exumbrella	Eurytele (510)	+++	12.92 ± 1.16	9.25 ± 0.94	8.99–16.19 × 5.93– 11.80	592.64 ± 159.29	175.71– 1077.70
			a-isorhiza (60)	++++	6.27 ± 0.65	3.53 ± 0.41	4.72–7.27 × 2.69–4.71	41.51 ± 11.04	23.28–79.40
			A-isorhiza*	rare to +	–	–	–	–	–
O-isorhiza (64)			absent to ++	21.99 ± 2.08	19.73 ± 2.17	17.87–26.07 × 15.31– 24.19	4619.10 ± 1409.00	2433.59– 7629.99	
Manubrium		Eurytele (46)	+++	13.28 ± 1.17	9.54 ± 0.82	10.50–15.36 × 7.42– 11.45	644.14 ± 155.14	302.99–993.32	
		a-isorhiza (53)	++++	6.69 ± 0.84	4.01 ± 0.54	5.18–8.02 × 3.05–5.39	58.69 ± 21.37	26.65–122.00	
		A-isorhiza (11)	absent to +	12.95 ± 0.61	7.79 ± 0.50	11.65–14.13 × 7.12– 8.63	414.60 ± 65.86	323.40–538.50	
		O-isorhiza (31)	absent to ++	19.80 ± 2.02	17.55 ± 2.56	15.32–23.56 × 12.80– 24.02	3332.99 ± 1194.03	1327.77– 6495.87	
Tentacles		Eurytele (44)	+++	12.69 ± 1.43	9.53 ± 1.34	10.2–16.71 × 7.27– 12.99	632.47 ± 262.44	304.97– 1476.59	
		a-isorhiza (107)	++++	5.88 ± 0.60	3.70 ± 0.45	4.39–7.70 × 2.99–5.65	43.42 ± 14.99	22.47–128.86	
	A-isorhiza (55)	absent to ++	14.27 ± 1.38	8.03 ± 0.62	12.51–18.62 × 6.51–9.54	488.81 ± 113.31	290.98–848.24		
	O-isorhiza (4)	absent to +	22.38 ± 0.55	20.65 ± 0.84	21.59–23.13 × 19.80– 21.96	5004.16 ± 404.93	4476.70– 5653.51		
Eurytele (112)	+++	14.07 ± 1.21	10.26 ± 0.86	10.72–17.98 × 7.82– 12.65	789.22 ± 185.84	343.08– 1357.32			

Abundance: nematocyst densities marked with increasing number + from one to four (+, ++, +++, +++++); absent, no nematocyst type found in investigated body parts; rare, nematocyst type not found in each investigated body part; exclusive, the only nematocyst type found in the investigated body part. SD, standard deviation. *Discharged nematocyst observed.

amount. Note differences in **Figures 4H,K** (red arrows). Near the rhopalial and velar canals and the central stomach, a clear nematocyst pattern appears (**Figures 4K, 6A**), with clusters of a-isorhizas and euryteles, but often some A-isorhizas and O-isorhizas (**Figure 5A**). Nematocyst clusters

are present in the incipient oral arms (**Figures 5B, 6D**) whereas random, scattered a-isorhizas are present in the manubrium base. A-isorhizas and O-isorhizas may be absent or present, but always in low abundances (**Figure 5B**). Marginal tentacles contain scattered a-isorhizas and euryteles

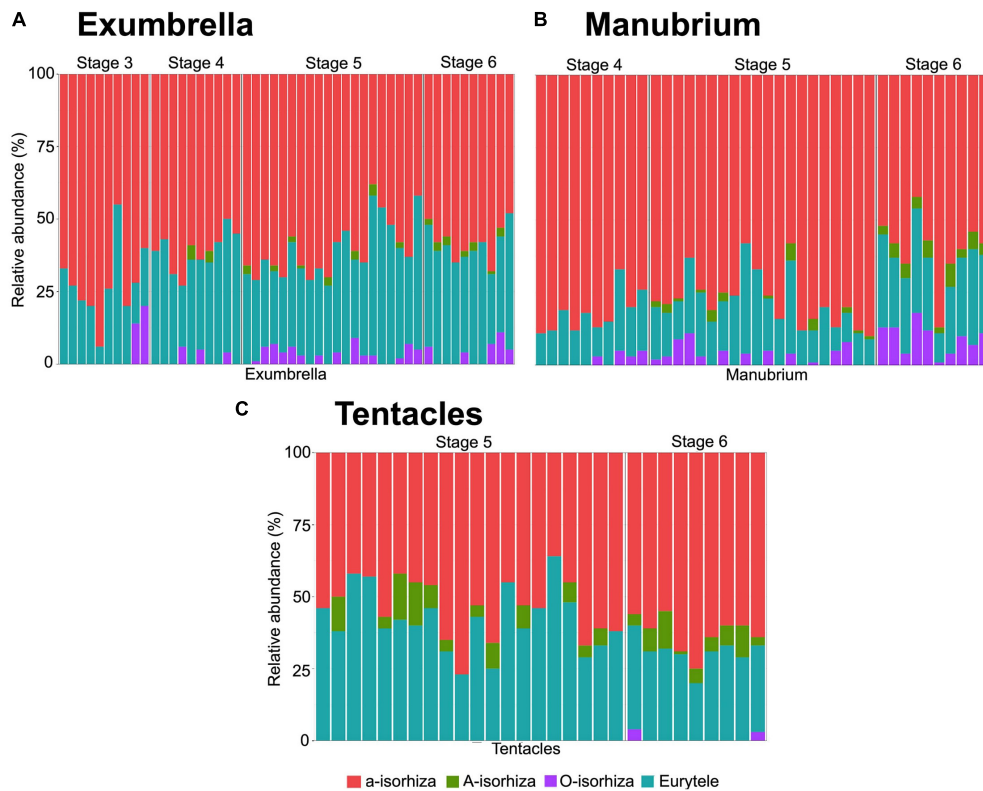


FIGURE 5 | Relative abundance of nematocyst types in batteries of different *Pelagia noctiluca* stages. **(A)** Exumbrella (50 batteries) **(B)** Manubrium (40 batteries). **(C)** Tentacles (30 batteries). Note large proportion of a-isorhizas and euryteles, and absence or very low proportion of A-isorhizas and O-isorhizas. Stages: metaephyra, stage 3; metaephyra, stage 4; juvenile medusa, stage 5; adult medusa, stage 6. Note: Gastric filaments not included due to the absence of nematocyst clusters.

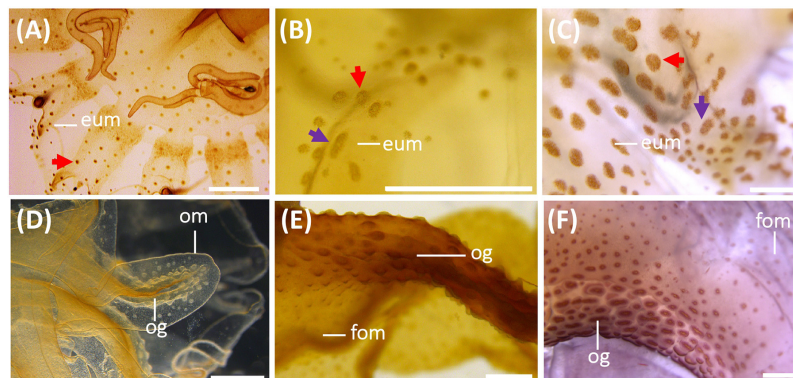


FIGURE 6 | Nematocyst batteries on exumbrella (eum) **(A–C)** and on oral arms **(D–F)** during the life cycle of *Pelagia noctiluca*. **(A,D)** Metaephyra, stage 4. **(B,E)** Juvenile medusa, stage 5. **(C,F)** Adult medusa, stage 6. **(A)** Homogenous, round-shaped batteries (red arrow). **(B,C)** Heterogeneous-shaped clusters, from round to oval (red arrow), narrow to oval-shaped (violet arrow). **(D–F)** High abundance of nematocyst warts throughout length of oral groove (og) compared to filled oral margin (fom). eum, exumbrella margin; fom, filled oral margin; om, oral margin; og, oral groove. Scale bars: 1 mm.

(Table 2). Euryteles are the only nematocyst type in the gastric filaments (Table 2).

Juvenile Medusa Stage

Stage 5 (Figure 8): The juvenile medusa stage displays a large TBD range (14.10–70.00 mm). As the medusae

grow, coloration changes, and young medusae turn intense brown. The nematocyst battery pigmentation appears less prominent due to less contrast between the brown medusa color and the brown nematocyst warts (Figures 6B,E). As the juvenile reaches the last medusa stage (Figures 6C,F), the intense brown coloration attenuates and the pigmented

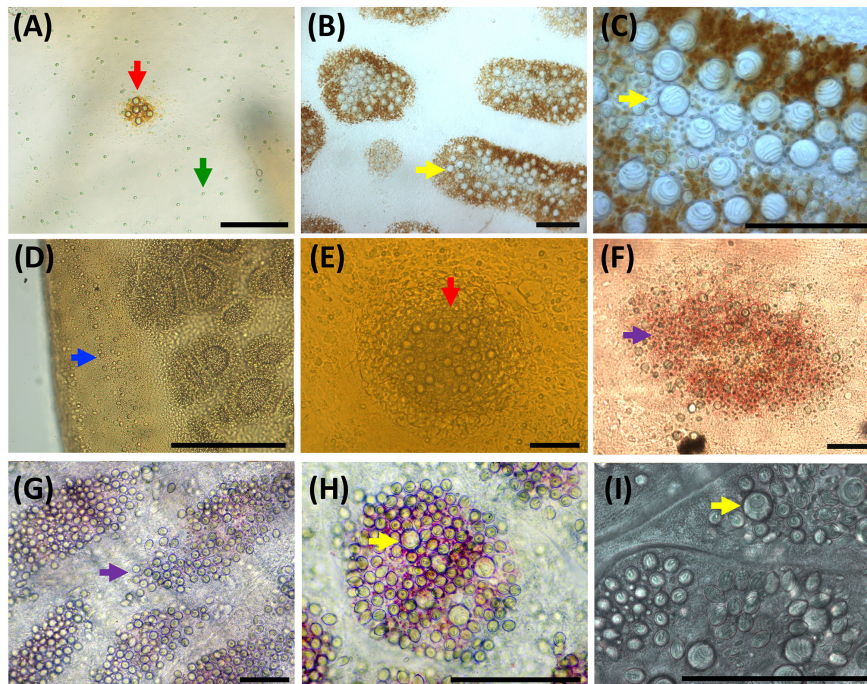


FIGURE 7 | Nematocyst clusters in different body parts. **(A–C)** Exumbrella. **(D–F)** Oral arms. **(G–I)** Marginal tentacles. **(A)** Abundant a-isorhizas (green arrow) randomly distributed despite initial nematocyst battery (red arrow) in metaephyra, stage 4. **(B,C)** Brown pigmented nematocyst batteries from adult medusa, stage 6. Note abundant O-isorhizas (yellow arrows). **(D)** Nematocyst line in rim of frilled oral margin (blue arrow) from juvenile medusa, stage 5. **(E,F)** Round (red arrow) to oval (violet arrow) nematocyst clusters in the oral groove from juvenile medusa, stage 5 **(E)** and adult medusa, stage 6 **(F)**. **(G–I)** Nematocyst batteries in marginal tentacles from adult medusa, stage 6. **(G)** Narrow to oval nematocyst batteries (violet arrow) with absence of large O-isorhizas. **(H,I)** Nematocyst batteries with presence of O-isorhizas (yellow arrows). Scale bars: 100 μm . **(G,H)** photographed by Rubén Duro.

nematocyst warts were more notable on the exumbrella and manubrium. Marginal tentacles are also brown. Rhopalial lappets have rounded tips.

Gastric system

Velar canals grow further into the marginal lappet, and they are completely at same level with the rhopalial canals. Rhopalial lappets continued to grow without formation of additional tentacular lappets. Each lappet contains a fork arm of the rhopalial canal and another of the velar canal. With growing size, the gastric pouches enlarge and widen in a centrifugal direction. Sixteen clearly visible unbranched, straight radial septa divide the gastrovascular cavity (**Figure 8**, ventral view). The marginal tentacles grow simultaneously and the margin of the oral arms are increasingly frilled. The gastric filaments increase in number and varies in length.

Cnidome

Nematocysts generally appear completely in clusters, but occasionally, some single and loosely scattered nematocysts are observed. In the exumbrella and oral arms, the composition of the nematocyst batteries is closely similar formed mainly of a-isorhizas and euryteles A-isorhizas and O-isorhizas may be present or absent (**Table 2** and **Figures 5A,B**). Warts are round to oval-shaped (**Figure 6B**, red arrow) and narrow to oval-shaped (**Figure 6B**, violet arrow). Throughout the oral groove, abundant nematocyst warts with oval and narrow to

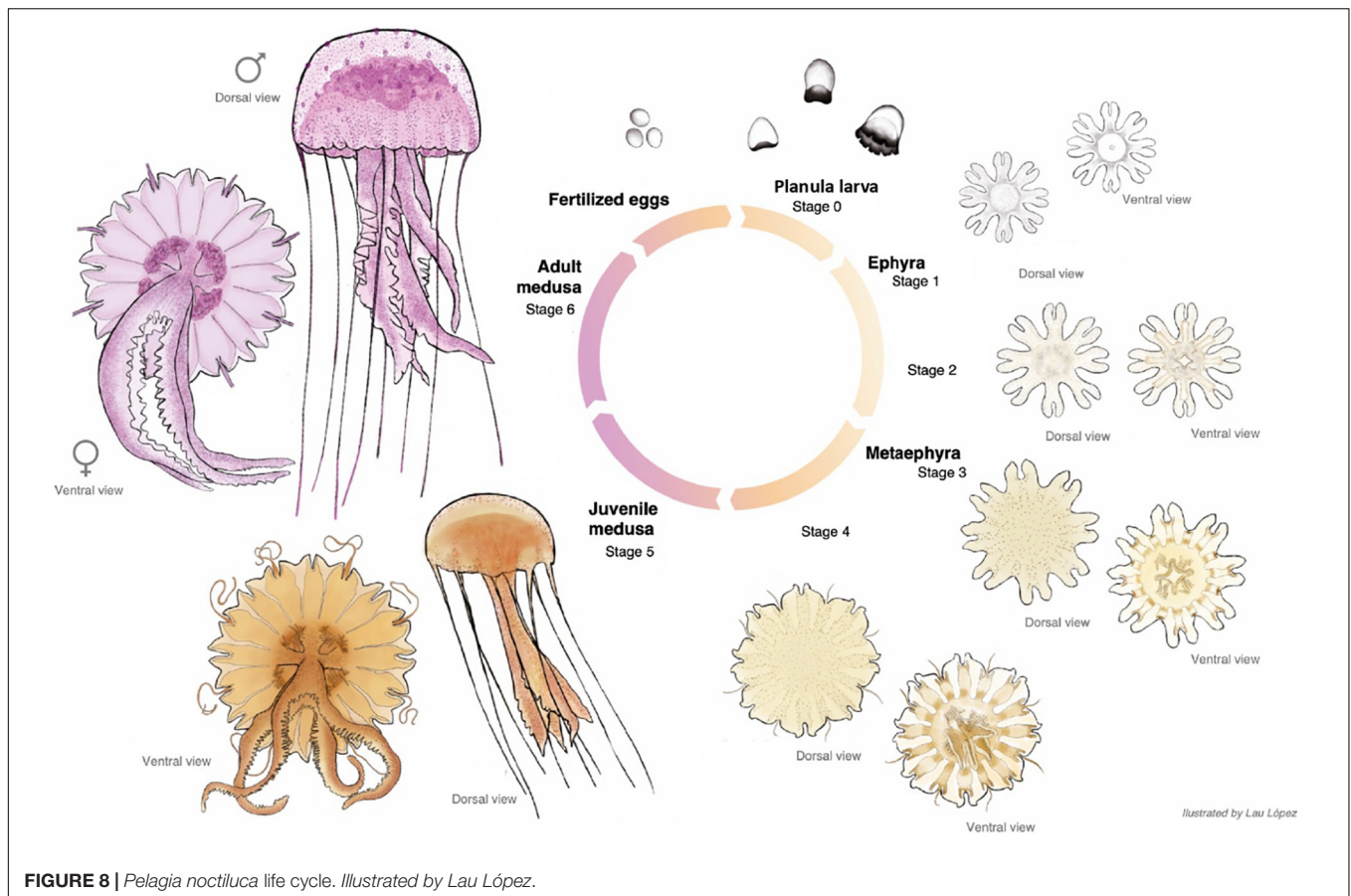
oval-shaped in comparison with the frilled oral arm margin, (**Figure 6E**) only with oval-shaped. A clear line of scattered a-isorhizas, A-isorhizas and euryteles are present at the rim of the oral groove and on the frilled margin (**Figure 7D**, blue arrow). Nematocyst batteries are present in high densities, covering a large proportion of tentacle areas; a-isorhizas and euryteles dominate. In comparison with other body parts A-isorhizas are highly abundant while O-isorhizas are present (always in low abundances) or absent (**Figure 5C**). The shape of the nematocyst warts varies throughout the tentacle. The shape of the nematocyst batteries varies throughout the tentacle. At the base, close to the umbrella, nematocyst batteries are round to oval-shaped while the narrow to oval-shaped cover the remaining marginal tentacle, including the tip.

Adult Medusa Stage

Stage 6 (Figure 8): Cultured adult medusae have a TBD range of 71.00–100.00 mm with the typical mauve to pink coloration. The gonads, along with the gastric filaments, occur in the four quadrants above the central stomach, and in alternation with the four oral arms (**Figure 8**, ventral view).

Gastric system

Rhopalial and velar canals grow in a centrifugal direction. No changes are noted compared to the most developed juvenile medusae.



Cnidome

The battery pattern, including presence of nematocyst types, is closely similar to the most developed juvenile medusae (Figures 6C,F, 7B,C,G–I). The clusters mainly consist of a-isorhizas and euryteles followed by some O-isorhizas and A-isorhizas. The relative abundance (RA) of the different nematocyst types is presented in Figure 5, and their measurements in Table 2.

Nematocyst Capsule Volume During the Life Cycle

A positive correlation (Pairwise test $p < 0.001$) is observed between increasing TBD and increasing capsule volume (CV) for all nematocyst types during the different developmental stages of *P. noctiluca* (Figure 9).

During the early stages, the mean CV of euryteles in the gastric filaments is larger than in the other parts of the body analyzed (Table 2 and Figure 10D). In metaephyra stage 4, the CV of euryteles from gastric filaments is significantly larger (Pairwise test $p < 0.001$) than in euryteles from exumbrella, manubrium and marginal tentacles.

The presence of A-isorhizas and O-isorhizas within the batteries varies widely, from present in low abundances to completely absent; with greater presence in advanced developed

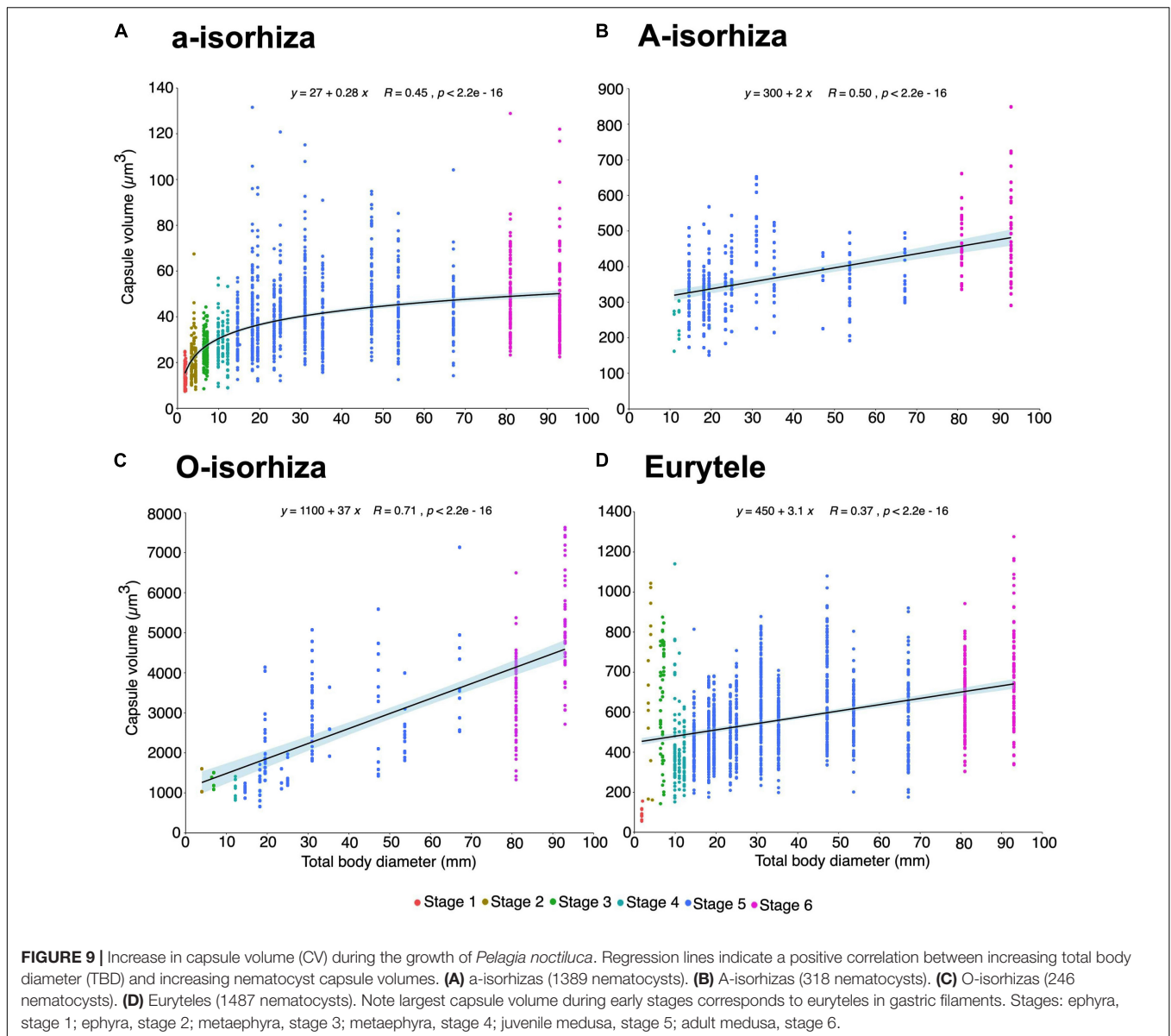
stages than in early stages contrary to a-isorhizas (Figures 10A–C). Although O-isorhizas first appear in ephyra stage 2, it is not until the juvenile stage 5 when their CV begins to increase (Partner test $p < 0.05$). In contrast, the CV of the A-isorhizas increases from their first observation in metaephyra stage 4 (Pairwise $p < 0.001$) (Table 2). The CV of the A-isorhizas present in the tentacles also increases with the growth of the jellyfish (Pairwise $p < 0.001$) (Figure 10B). Full statistical data are presented in Supplementary Material.

DISCUSSION

Nematocyst Identification

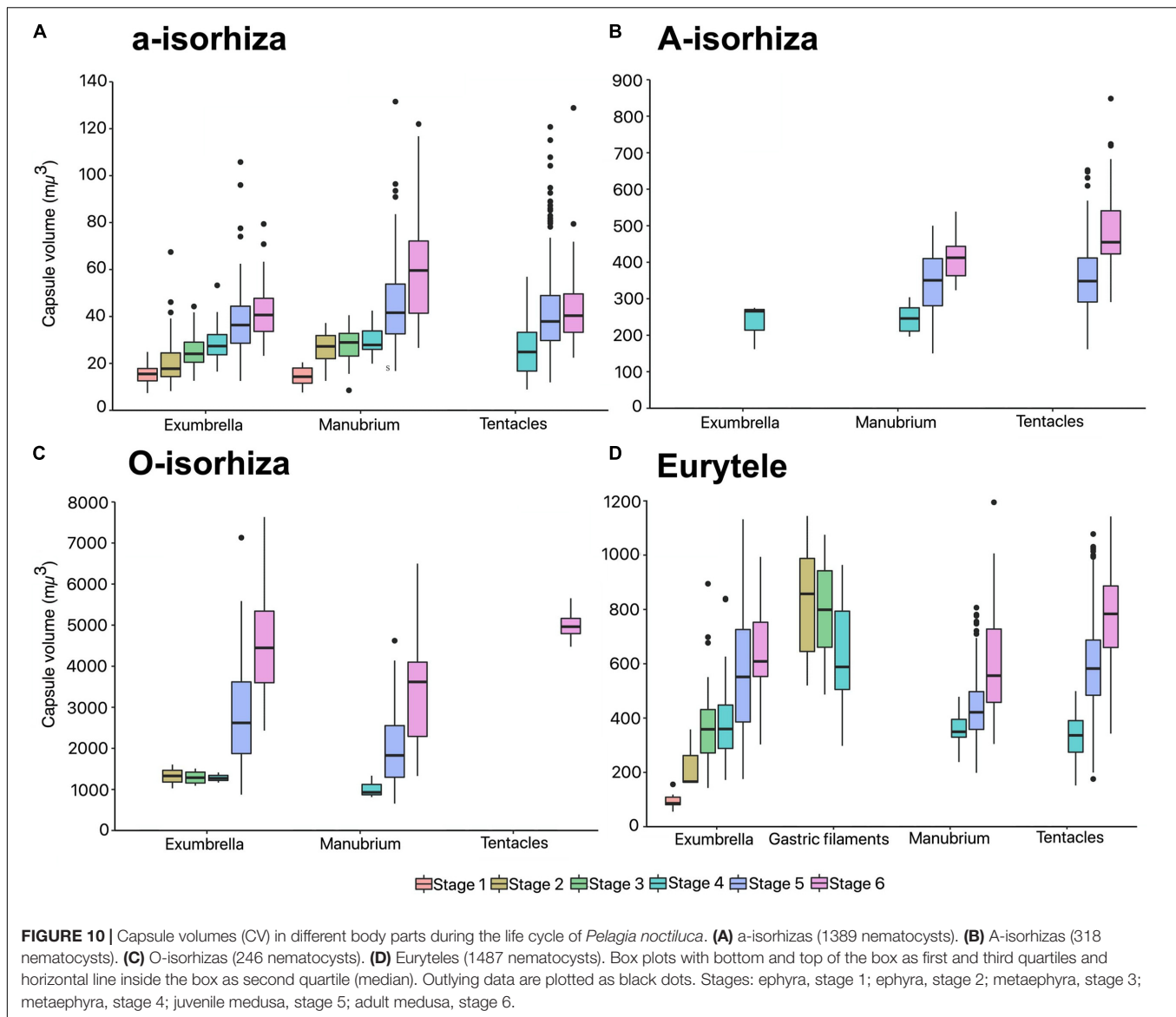
Improvements in microscopic observation techniques have changed the criteria for nematocyst classification. It is therefore essential to re-examine, identify and classify them. In our study, four nematocyst types were identified during the life cycle of *P. noctiluca*: (I) homotrachous a-isorhiza, (II) homotrachous A-isorhiza, (III) homotrachous O-isorhiza and (IV) heterotrachous microbasic eurytele.

In the present study, the previously termed atrichous isorhizas (Krasinska, 1914; Weill, 1934; Avian et al., 1991) of *P. noctiluca* are reclassified as homotrachous a-isorhizas (Figure 2A) in accordance with Östman (1991) and Östman and Hydman (1997). Although no discharged a-isorhiza were examined



in detail here, the discharged a-isorhizas showed prominent homotrichous spines on the proximal tubule in *Cyanea capillata* (Östman and Hydman, 1997, e.g., Figures 1 and 21G and 21I). The previously termed atrichous isorhizas (Krasinska, 1914; Weill, 1934) and heterotrichous isorhizas (Avian et al., 1991) are reclassified as homotrichous A-isorhizas (Figure 2B) in line with the A-isorhizas, which showed weak, slender spines of the same size along most of the discharged tubules, in *A. aurita* (Östman, 1991) and *C. capillata* (Östman and Hydman, 1997, e.g., Figures 22 and 23). Herein, the A-isorhiza tubules were not examined in detail. The previously termed holotrichous isorhizas (Krasinska, 1914; Weill, 1934; Avian et al., 1991) are reclassified as homotrichous O-isorhizas (Figure 2A), in accordance with Östman and Hydman (1997) (E.g., Figures 3 and 24), based on our observations of the regular pattern of spines in three helical rows on the proximal and mid-tubule (Figure 2G).

Confirming previous identifications, heterotrichous microbasic euryteles are found in *P. noctiluca* (Krasinska, 1914; Weill, 1934; Larson, 1987; Avian et al., 1991). Recently, some authors have suggested that undischarged euryteles are often indistinguishable from undischarged birhopaloid type II nematocysts (shaft with two dilatations) (Morandini and Marques, 2010; Heins et al., 2015), first identified by Östman and Hydman (1997). For this reason, some studies have encompassed eurytele and birhopaloid type II nematocysts into rhopaloid nematocysts (shaft with unequal diameter) (Morandini and Marques, 2010; Heins et al., 2015; Ames et al., 2020). Discharged shafts of euryteles have a single distal dilatation (Östman and Hydman, 1997, e.g., Figures 4 and 25), whereas discharged shafts of birhopaloid type II have two dilatations close together (Östman and Hydman, 1997, e.g., Figures 5 and 26). These shaft differences were clearly shown in LM



(Östman and Hydman, 1997, e.g., Figures 25E and 26D) and not only in SEM. In the present study, nematocysts with a shaft with one dilatation armed with prominent spines, distal to a narrow, straight spineless shaft, are referred to as euryteles (**Figures 2H,I**). We therefore confirm that euryteles are the only nematocyst present within the rhopaloid category for *P. noctiluca*; there no birhopaloid II nematocysts were identified in LM. The LM technique was also successfully used to identify the dilatations of eurytele and birhopaloid in *Cassiopea andromeda* (Heins et al., 2015, e.g., Figure 3J). As described by Östman and Hydman (1997), euryteles have large prominent spines on the distal shaft dilatation, and the distal tubule is armed with spines in clear triple helices. The hook-shaped spine pattern on the distal tubule (Östman and Hydman, 1997, e.g., Figure 25D) was not visible in our LM photos.

An unknown type described as a nematocyst with a fusiform, flat to slightly curved capsule was identified in *P. noctiluca*

specimens by Avian et al. (1991). This nematocyst type was not documented and it was considered a preliminary result (Avian et al., 1991). Generally, nematocyst capsules of Scyphozoa (Medusozoa) are broad, rounded to sub-spherical or broad elongated, not narrow elongated with the typical capsule shape as in sea anemones (Anthozoa) (Östman, 2000, e.g., Figure 2). The common, typical, elongated b-mastigophore and p-mastigophore nematocysts of actiniarian species (Östman, 2000 e.g., Figure 2; Östman et al., 2010a,b), or the shorter, less common hydrozoan b-mastigophores (Östman, 1989, e.g., Figure 3) have to date not been identified in scyphozoans. However, Yue et al. (2020) reported b-mastigophores within the jellyfish *Cyanea nozakii*, which we, based on their tubule pattern and lost spines, doubt are similar to the common actiniarian and hydrozoan b-mastigophores. Avian et al. (2016) (e.g., Figure 10H) described a new nematocyst, a possible p-mastigophore, for the Mediterranean jellyfish *Mawia benovici* (Pelagiidae), previously

described as *Pelagia benovici* [Piraino et al., 2014; WoRMS (World Register of Marine Species), 2020]. The nematocyst had an elongated, ellipsoid capsule, with shaft length almost equal to the capsule length (Avian et al., 2016), but no visible v-notch at the shaft end, characteristic for p-mastigophores (Strömberg and Östman, 2017, e.g., Figures 9B,C). In this study nematocysts with these morphological characteristics have not been identified.

Morphology Throughout the Life Cycle

Living cultures enable identification of nematocyst development and offer an irreplaceable opportunity to study, in detail, every step of the life cycle of *P. noctiluca*. Although strobilation is the most common mechanism by which scyphozoan ephyrae are formed, at least 4 species within Scyphozoa, including *P. noctiluca*, have lost or highly modified the planula or benthic phase of their life cycle (Jarms, 2010; Helm, 2018). The planula larva stage of *P. noctiluca* was described from laboratory conditions (Rottini Sandrini and Avian, 1983; Helm et al., 2015; Ramondenc et al., 2019). The development begins when the asymmetric planula becomes a “four-prong larvae” with four buds. As development progresses, the larva expands orally, and is recognized as a cone larva (Ramondenc et al., 2019, e.g., Figure 8). Four additional buds are formed between the previous four buds. Each bud transforms into a pair of rhopalial lappets with a nested rhopalium. Lastly, the cone larva is flattened and gives rise to the youngest ephyrae (Helm et al., 2015, e.g., Figure 1; Helm, 2018, e.g., Figure 8). In the present study, only the phase cone larva was observed.

To date, little is known about the development of the early ephyrae stages of *P. noctiluca*. Their descriptions and drawings can be consulted in Uchida (1934) as *Pelagia panopyra*, a former synonym of *P. noctiluca*, and in Russell (1970). Individuals about 2 mm in length (Uchida, 1934) and about 3.5 mm in length (Russell, 1970) were interpreted as ephyrae newly developed from planulae. Strangely, judging by the drawings, these ephyrae seemed to be transitions between ephyrae and metaephyrae (Table 1). In present ephyra stages, the velar canals are absent (stage 1) or present and spade-shaped (stage 2), in contrast to metaephyra stages, when they are forked and reach the umbrella rim (Table 1 and Figure 3). In addition, the rhopalial canals were forked (Uchida, 1934; Russell, 1970), but here they are unforked in ephyrae and forked in metaephyrae, differentiating ephyrae between metaephyrae (Table 1 and Figure 3). The absence of velar canals and gastric filament, and unforked rhopalial canals (Table 1 and Figures 3A, 4A) are important features for the identification of a newly developed *P. noctiluca* ephyra. The studies by Uchida (1934) and Russell (1970) were previously taken to be complete descriptions of ephyra development to young medusa, but the present investigation shows that they did not include all early stages.

The extensive and detailed information on morphological characteristics herein has made it possible to compare the youngest *P. noctiluca* ephyrae (holoplanktonic life cycle) with the well-known ephyrae, newly released from scyphopolyps (metagenetic life cycle), present in the Mediterranean basin (Table 3). Morphological studies in species such as *Rhizostoma*

luteum, *R. pulmo*, *C. tuberculata* and *A. aurita* reported the presence of velar canals with different shapes in newly released ephyrae (Table 3). However, we found the formation of spade-shaped velar canals in ephyra stage 2 of *P. noctiluca* (Table 1). Since velar canals are absent in newly developed ephyrae of *P. noctiluca* (Figures 3A,B), the presence or absence of velar canals in the first stage of ephyra may represent a differentiating characteristic between scyphozoan species with holoplanktonic or metagenetic life cycles.

The family Pelagiidae is composed of the well-known genera *Pelagia*, *Chrysaora*, *Sanderia* and the new, recently incorporated genus *Mawia* [Avian et al., 2016; WoRMS (World Register of Marine Species), 2020]. In contrast to *P. noctiluca*, species such as *Chrysaora fuscescens* and *Chrysaora lactea* develop a set of secondary tentacle sprouts at the marginal corners of the velar canals during the early ephyra stages. In *C. lactea*, tertiary tentacles are located between primary or secondary tentacles, splitting the tentacular lappet into two parts (Straehler-Pohl et al., 2011). In the scyphozoan family Cyaneidae, secondary and tertiary tentacles have been identified (Straehler-Pohl et al., 2011). Previous morphological descriptions of *P. noctiluca* ephyrae (Uchida, 1934; Russell, 1970; Ramondenc et al., 2019) indicated the presence of primary and secondary tentacles. However, our investigation affirms, for the first time, that *P. noctiluca* has only one set of primary tentacles, all growing nearly simultaneously (Figures 3G,H). Admittedly, some tentacles can develop a little faster than others, hence the description “nearly simultaneously,” which has already been used for *Chrysaora hysoscella* (Holst, 2012).

The different morphology and colors of adult Mediterranean jellyfish facilitate their identification (Holst, 2012; Marambio et al., 2021a). Russell (1970) described exhaustively the morphology of juvenile and adult medusae. The present description confirms his findings and high-resolution photographs have provided new details for both early and more advanced stages (Figures 3, 4, 6, 7).

The Cnidome and the Nematocyst Role Throughout the Life Cycle

The Mediterranean ephyrae of scyphozoan species are well-known morphologically; nevertheless, the majority of their descriptions are not accompanied by detailed information about their cnidome (Table 3). This study is the first to provide information about the cnidome of *P. noctiluca*, showing the different nematocyst sizes and patterns of distribution during the life cycle.

During the planula larva stage, the presence of a-isorhizas is observed on the cone larvae (Table 2), as in investigations of planulae from different cnidarian species (Martin and Chia, 1982; Calder, 1983; Holst et al., 2007; Yuan et al., 2008; Strömberg et al., 2019). However, it was not possible to measure their capsule volumes. An exhaustive analysis of each planula phase is suggested for future investigations.

The morphological descriptions by Uchida (1934) and Russell (1970) were accompanied by some information about the *P. noctiluca* cnidome. Uchida (1934) described conspicuous

TABLE 3 | Morphology including cnidome of scyphozoan ephyrae present in the Mediterranean Sea.

Species	Culture (T°)	TBD (mm)	CDD (mm) and body proportions	N° of marginal lappets	Lappet proportions: LStL/RLL of TMLL	Rhopalial/velar lappets. Gastric filaments per quadrant	Gastric system. Zooxanthellae	Color	Cnidome	References
<i>Pelagia noctiluca</i> *	18°C	3.38–4.89, mean: 4.00	1.61–2.27, mean: 1.91 39% of TBD	8	50%/50% of TMLL	Rhopalial lappets oval spoon- to bread knife-shaped. 1–3 gastric filaments	Rhopalial canals unforked, spade-shaped to slightly forked, round tips; velar canals unforked, spade-shaped. Zooxanthellae absent	Transparent and brown to ocher-colored in some areas	a-isorhizas abundant scattered, some euryteles and O-isorhizas over whole exumbrella. No nematocyst batteries	Present study
<i>Aurelia aurita</i>	15–25°C	3.86–4.50, mean: 4.19	1.44–1.81, mean: 1.66 40% of TBD	8	52%/48% of TMLL	Rhopalial lappets broad lancet-shaped. 1–2 gastric filaments	Rhopalial canals spade-shaped to slightly forked; velar canals rhombic. Zooxanthellae absent	Milky to bluish	–	Straehler-Pohl and Jarms (2010)
<i>Cassiopea andromeda</i>	25–28°C	3.69–3.95, mean: 3.79	2.43–2.69, mean: 2.56 68% of TBD	17–23, mean: 19	48%/52% of TMLL	Rhopalial lappets spatula-shaped; rhopalial and velar lappets connected by a thin lamella. 16–21 (mean: 18) velar lappets. Gastric filament absent	Rhopalial canals long, forked, round tips, nearly totally filled rhopalial lappet; velar canals unforked, spatula-shaped, nearly filled velar lappet. Zooxanthellae present	Yellowish green	–	Straehler-Pohl and Jarms (2010)
<i>Catostylus mosaicus</i>	20°C	1.90–2.66, mean: 2.11	0.88–0.94, mean: 0.93 44% of TBD	8	56%/44% of TMLL	Rhopalial lappets antler/palm-shaped with finger like appendages. 1–2 gastric filaments	Rhopalial canals slightly forked, sharp-sharped tips; velar canals unforked, spade-shaped. Zooxanthellae absent	Milky transparent	8 long nematocyst batteries along arms of marginal lobes, 8 circular batteries around manubrium	Straehler-Pohl and Jarms (2010)
<i>Chrysaora hysoscella</i>	10–15°C	2.84–3.40, mean: 3.18	1.18–1.42, mean: 1.32, 42% of TBD	8	45%/55% of TMLL	Rhopalial lappets round, spatula-shaped. Gastric filament absent	Rhopalial canals forked, sharp-shaped tips; velar canals forked, sharp-shaped tips. Zooxanthellae absent	Rose	–	Straehler-Pohl and Jarms (2010)
<i>Cotylorhiza tuberculata</i>	25–28°C	2.72–3.25, mean 2.99	1.10–1.49, mean: 1.27 42% of TBD	8	61%/39% of TMLL	Rhopalial lappets round spoon-shaped. 1 gastric filament per quadrant	Rhopalial canals slightly forked, round-shaped tips; velar canals unforked, spade to slightly rhomboid-shaped. Zooxanthellae mark gastric system line	Transparent with yellow hemmed gastric system	–	Straehler-Pohl and Jarms (2010)
<i>Nausithoe weneri</i>	20–23°C	0.65–0.66	0.37–0.38, mean: 0.38 56–58% of TBD	16	0%/100% of TMLL	Rhopalial lappets round, spoon-shaped. Gastric filament absent	Very short gastric canal-like protuberances of central stomach reach marginal lappet base. Zooxanthellae present	Transparent, with muscle ring	–	Straehler-Pohl and Jarms (2010)
<i>Rhizostoma luteum</i>	23°C	3.41–4.52, mean 4.01	Mean: 2.39, 60% of TBD	8	50%/51% of TMLL	Rhopalial lappets bread knife-shaped; rhopalium directly attached to central disk. 3–7 gastric filaments	Rhopalial canals slightly forked, sharp-shaped tips; velar canals forked, flat rhombic tips. Zooxanthellae absent	Light mustard to dark gold	Nematocyst warts scattered over exumbrella	Kienberger et al. (2018)

(Continued)

TABLE 3 | Continued

Species	Culture (T°)	TBD (mm)	CDD (mm) and body proportions	N° of marginal lappets	Lappet proportions: LStL/RLl of TMLL	Rhopalia/velar lappets. Gastric filaments per quadrant	Gastric system. Zooxanthellae	Color	Cnidome	References
<i>Rhizostoma pulmo</i>	21°C	2.28–3.93, mean: 3.17	0.96–1.62, mean: 1.35 43% of TBD	8	56%/44% of TMLL	Rhopalial lappets spade to lancet-shaped. 2–4 gastric filaments	Rhopalial canals forked; velar canals unforked, diamond-shaped. Zooxanthellae absent	Opaque white	Small, white nematocyst clusters scattered over whole exumbrella	Fuentes et al. (2011)
<i>Rhopilema nomadica</i>	20°C	1.5–2.0	50% of TBD	8	53% ^P /47% ^P of TMLL	Rhopalial lappets single or twin-typed, lancet-shaped. Gastric filaments absent	Distal end of each rhopalial canal is convex with arched corners on both sides	–	Nematocyst batteries on exumbrella, arranged in two whorls, inner one on bell and outer one on lappets, on both sides of each rhopalial canal	Lotan et al. (1992)
<i>Phyllorhiza punctata</i>	25–28°C	0.46	Mean: 0.22 48% of TBD	8	67%/33% of TMLL	Rhopalial lappets pointed, spoon-shaped. 0–1 gastric filament	Rhopalial canals slightly forked, round tips, velar canals unforked, spade to slightly rhomboid-shaped. Zooxanthellae present	Ocher. White spots on exumbrella	–	Straehler-Pohl and Jarms (2010)

CDD, central disk diameter; LStL, lappet stem length; RLl, rhopalial lappet length; SD, standard deviation; TBD, total body diameter; TMLL, total marginal lappet length; TMlL, total marginal lappets length; *morphological and cnidome descriptions for ephyra stage 2 of *Pelagia noctiluca*.

nematocyst clusters on the whole surface of a newly developed ephyra from a planula of *P. noctiluca*, and Russell (1970) described, from a *P. noctiluca* ephyra measuring 3.5 mm (close to our present ephyra stage 2, **Table 1**), warts in a regular pattern as a useful identification characteristic for ephyrae. Contrary to their findings, we observe the presence of nematocyst clusters in individuals belonging to metaephyra stage 3 (size range 5.10–8.00 mm. **Table 1** and **Figure 4H**), which are absent in younger ephyrae (**Figures 4B,E**).

Nematocyst batteries in scyphopolyps and in newly released ephyrae have been identified in numerous scyphozoan studies (Kikinger and von Salvini-Plawen, 1995; Schiariti et al., 2008; Widmer, 2008; Fuentes et al., 2011; Kienberger et al., 2018). The absence of nematocyst batteries in the younger ephyrae of *P. noctiluca*, with a holoplanktonic life cycle, could suggest that the nematocyst battery pattern is acquired during the strobilation process in metagenetic life cycles, being a feature transferred from scyphopolyps to newly released ephyrae. The delayed nematocyst battery formation in *P. noctiluca* is probably associated with its holoplanktonic life cycle.

The different nematocyst types and their appearance during the life cycle have been linked with dietary variations, preferred prey item and prey capture (Purcell, 1984; Purcell and Mills, 1988; Östman and Hydman, 1997, Jarms et al., 2002; Heins et al., 2015). A variety of prey was identified in the gut contents of *P. noctiluca* (Sabatés et al., 2010; Tilves et al., 2016), which might explain the different nematocyst sizes and their distribution throughout the life cycle observed in our study. In accordance with previous research in scyphozoans (Östman and Hydman, 1997; Jarms et al., 2002; Heins et al., 2015), our investigation reinforces the existence of a positive correlation (Pairwise test $p < 0.001$) between increased nematocyst size and increased body diameter throughout the life cycle (**Figure 9**). The capacity to capture larger prey could, according to Jarms et al. (2002) and Heins et al. (2015), explain the increasing nematocyst size throughout the *P. noctiluca* life cycle.

In the early developmental stages, copious amounts of a-isorhizas are randomly distributed in the ectoderm, and are still present even when the first nematocyst batteries appeared in metaephyrae (**Figure 4H**). During the growth of young juvenile medusae, single randomly scattered nematocysts are less common and nematocyst clusters become more common. The present investigation highlights, for the first time, that a complete aggregation of nematocysts in batteries is a gradual process during the life cycle of *P. noctiluca*. A complete battery distribution is not related to the preference of a specific food item, since *P. noctiluca* is an opportunistic predator (Milisenda et al., 2018), but with the ability to capture larger prey and ingest more food. Many nematocysts discharge simultaneously and eject abundant parallel-oriented tubules (**Figure 2F**), thus operating more efficiently than a single nematocyst, according to Östman and Hydman (1997) (e.g., **Figures 30F** and **30G**). The drawings by Russell (1970) showed the distribution and shapes of the nematocyst batteries from adult *P. noctiluca* medusae. The findings of Russell (1970) are validated here, and high-resolution photographs of the cnidome are provided (**Figures 6, 7**).

In line with our findings, previous authors have reported that a-isorhizas and euryteles were common in several scyphozoan species (Calder, 1971, 1977, 1983; Östman and Hydman, 1997; Jarms et al., 2002; Morandini and Marques, 2010; Heins et al., 2015; Ames et al., 2020; Killi et al., 2020). The great abundance of a-isorhizas and euryteles in different body parts of *P. noctiluca* specimens (Table 2) prove their important roles throughout the life cycle. The large proportions of a-isorhizas and euryteles described here (Figure 5) suggest their main functions to be prey capture and defense against predators (Mariscal, 1974). The abundance of euryteles linked to the formation of nematocyst batteries (Table 2) reveals an important function in the more developed stages. Spines are clearly identified on the eurytele distal shaft dilatation (Figures 2H,I), supporting their previously reported penetrating function (Östman and Hydman, 1997; Purcell, 1984).

The presence of euryteles in gastric filaments has been reported for cnidarian species (Jarms et al., 2002; Morandini et al., 2004; Di Camillo et al., 2006). Their exclusivity in *P. noctiluca* gastric filaments proves successful prey capture in the early ephyra stages. The large volume of the eurytele capsule is fundamental, making it possible to store large volumes of toxins (Table 2) when structures such as marginal tentacles, specialized for prey capturing, are absent or not completely developed in early stages (Figures 3A–F). In *P. noctiluca* adult medusae, Larson (1987) reported the presence of atrichous nematocysts in gastric filaments, but the gastric filaments of advanced stages were not analyzed in our study. Future investigation is suggested to find out if the atrichous nematocysts (Larson, 1987) are identical to the euryteles found in our *P. noctiluca* early stages (Table 2).

It is known that changes in the cnidome occur during the strobilation process (Calder, 1973). New nematocyst types, such as O-isorhizas and A-isorhizas, unlike a-isorhizas and euryteles, were added during polyp fission and described for the first time in the strobilae or newly released ephyrae of some species (Calder, 1973, 1977; Morandini et al., 2004, 2006; Heins et al., 2015; Ames et al., 2020). A-isorhiza and O-isorhiza are more common in advanced stages of the life cycle of *P. noctiluca* (Table 2). Their intermittent presence observed here indicates a complementary role to the highly abundant a-isorhizas and euryteles in the advanced stages (Figure 5). Heins et al. (2015) suggested that the presence of A-isorhizas and O-isorhizas in the life cycle was an adaptation to the change in prey preference associated with progress through developmental stages. On the contrary, the presence of A-isorhizas and O-isorhizas is probably related to the ability to capture larger prey than in the early stages because *P. noctiluca* is considered a non-selective predator (Milisenda et al., 2018). Östman and Hydman (1997) (e.g., Figure 30) showed that several A-isorhiza tubules in a bundle, only armed with small, slender spines without hooks, entangled and anchored the prey. Their adhesive capacity could explain their increased abundance in tentacular batteries, reported here (Table 2). The presence of penetrating O-isorhizas on the exumbrella and oral arms of *P. noctiluca* (Figures 5A,B) is certainly linked to defense against predators, but also to prey capture, since, apart from the oral arms and marginal tentacles,

food can also be captured and transported by the exumbrella (Larson, 1987).

The Nematocyst Effect on Human Health

In the Mediterranean basin, *P. noctiluca* is considered a highly venomous jellyfish with negative effects on human health (Mariottini et al., 2008; Canepa et al., 2014; Marambio et al., 2021a). The contribution of the toxicological properties of each nematocyst in the sting is difficult to determine in jellyfish species (Doyle et al., 2017). However, the cytotoxic capacity from *P. noctiluca* isolated euryteles has been reported by Morabito et al. (2020). Besides the toxic properties of the venom, the length of the nematocyst tubule leads to varying degrees of epithelial damage (Kitatani et al., 2015). The eurytele has longer tubules (mean 570.05 μm) (Avian et al., 1991) than isorhizas (Figure 2), and together with the shaft dilatation armed with prominent spines (Figures 2H,I), penetrates the human skin epidermis and stimulates free nerve endings in the subepidermal plexus, leading to pain (Kitatani et al., 2015). Despite the absence of shaft (Figures 2F,G) and the low abundance of O-isorhizas in batteries (Figure 5), the large capsule volume for storing venom (Table 2), together with a long tubule (mean 470.51 μm) (Avian et al., 1991), plays an important role in the *P. noctiluca* stings. The small a-isorhiza, with tubules shorter than 200 μm (Avian et al., 1991), could be involved to a lesser degree in the injection of toxins. In *C. capillata*, A-isorhiza does not have a penetrating function (Östman and Hydman, 1997), possibly excluding its involvement in the sting mechanism.

The stinging water phenomenon caused by cassiosomes, an outer epithelial layer mainly composed of nematocysts, had been described as a major cause of stings in bathers and aquarists interacting with jellyfish of the Order Rhizostomeae (Ames et al., 2020). However, our findings show that even in the absence of cassiosomes – a rhizostome evolutionary novelty – threat of envenomation by *P. noctiluca* (Order Semaestomeae) can unsuspectedly occur due to an abundance of early life stages present in the water, and is not linked solely to advanced stages.

CONCLUSION

Pelagia noctiluca is one of few scyphozoans with a holoplanktonic life cycle. During its early development, 4 stages are identified (ephyra stage 1, ephyra stage 2, metaephyra stage 3 and metaephyra stage 4). Four nematocyst types are identified during the life cycle: a-isorhiza, A-isorhiza, O-isorhiza and eurytele. The first nematocyst clusters appear in the metaephyra stage 3. The pattern of nematocysts exclusively in batteries occurs gradually. The nematocyst number and capsule volume increase with increasing body diameter. The a-isorhizas and euryteles are present in all batteries; A-isorhizas and O-isorhizas are complementary nematocysts, having important roles in prey capture in the more developed stages. Euryteles on the gastric filaments during the early stages are larger than those of the exumbrella, showing the importance of the increased capsule volume when marginal tentacles, specialized for feeding, are

not fully developed. Increased capsule volume and increased nematocyst aggregation enable more and longer tubules and more toxins to be released simultaneously, allowing large prey to be captured. O-isorhizas and euryteles are the main nematocysts causing serious stings in beach users. Therefore, as scientific community strive to develop safe guidelines and first aid protocols for addressing mauve stinger envenomation, the focus should be on developing a substance that inhibits discharge of O-isorhizas and eurytele nematocysts as a potential countermeasure to stings from this species.

DATA AVAILABILITY STATEMENT

The original contributions presented in the study are included in the article/ **Supplementary Material**, further inquiries can be directed to the corresponding author/s.

AUTHOR CONTRIBUTIONS

AB conceived the study, designed the experiment, collected the jellyfish, supervised the jellyfish cultures, collected and analyzed the data, and wrote and edited the manuscript. CÖ participated in the analysis of results and the writing of the manuscript. AS contributed to the experimental design, performed the statistical analyses, and drew up the graphs. MM participated in the experimental design. CÖ, AS, MM, MN, and J-MG revised the

manuscript and contributed to its improvement. All authors approved the submitted version.

FUNDING

Supported by the ISDIN project. This study is part of an Industrial Doctorate program.

ACKNOWLEDGMENTS

We greatly appreciate the participation of Carlos Mengod in the collection of jellyfish. AB was supported by a grant awarded by AGAUR (Agència de Gestió d'Ajuts Universitaris i de Recerca), which allowed presentation of the preliminary results of the present study in the 6th Jellyfish Bloom Symposium (Cape Town, South Africa). We acknowledge the 'Severo Ochoa Center of Excellence' accreditation (CEX2019-000928-S). Finally, we want to thank to the reviewers for their valuable comments and suggestions to improve the manuscript.

SUPPLEMENTARY MATERIAL

The Supplementary Material for this article can be found online at: <https://www.frontiersin.org/articles/10.3389/fmars.2021.714503/full#supplementary-material>

REFERENCES

- Al-Rubiay, K. K., Al-Musaoui, H. A., Alrubaiy, L., and Al-Freje, M. J. (2009). Skin and systemic manifestations of jellyfish stings in Iraqi fishermen. *Libyan J. Med.* 4, 75–77. doi: 10.4176/081215
- Ames, C. L., Klompen, A. M., Badhiwala, K., Muffett, K., Reft, A. J., Kumar, M., et al. (2020). Cassiosomes are stinging-cell structures in the mucus of the upside-down jellyfish *Cassiopea xamachana*. *Commun. Biol.* 3:67. doi: 10.1038/s42003-020-0777-
- Avian, M., Del Negro, P., and Rottini Sandrini, L. (1991). A comparative analysis of nematocysts in *Pelagia noctiluca* and *Rhizostoma pulmo* from the North Adriatic Sea. *Hydrobiologia* 216, 615–621. doi: 10.1007/BF00026521
- Avian, M., Ramšak, A., Tirelli, V., D'Ambra, I., and Malej, A. (2016). Redescription of *Pelagia benovici* into a new jellyfish genus, *Mawia*, gen. nov., and its phylogenetic position within Pelagiidae (Cnidaria: Scyphozoa: Semaestomeae). *Invertebr. Syst.* 30, 523–546. doi: 10.1071/IS16010
- Ballesteros, A., Marambio, M., Fuentes, V., Narda, M., Santín, A., and Gili, J. M. (2021). Differing effects of vinegar on *Pelagia noctiluca* (Cnidaria: Scyphozoa) and *Carybdea marsupialis* (Cnidaria: Cubozoa) stings—implications for first aid protocols. *Toxins* 13:509.
- Brotz, L., Cheung, W. W. L., Kleisner, K., Pakhomov, E., and Pauly, D. (2012). Increasing jellyfish populations: trends in large marine ecosystems. *Hydrobiologia* 690, 3–20. doi: 10.1007/978-94-007-5316-7_2
- Brotz, L., and Pauly, D. (2012). Jellyfish populations in the Mediterranean Sea. *Acta Adriat.* 53, 213–232.
- Calder, D. R. (1971). Nematocysts of polyps of *Aurelia*, *Chrysaora*, and *Cyanea*, and their utility in identification. *Trans. Am. Microsc. Soc.* 90, 269–274. doi: 10.2307/3225186
- Calder, D. R. (1973). Laboratory observations on the life history of *Rhopilema verrilli* (Scyphozoa: Rhizostomeae). *Mar. Biol.* 21, 109–114. doi: 10.1007/BF00354606
- Calder, D. R. (1974). Nematocysts of the coronate scyphomedusa, *Linuche unguiculata*, with a brief reexamination of scyphozoan nematocyst classification. *Chesapeake Sci.* 15, 170–173. doi: 10.2307/1351039
- Calder, D. R. (1977). Nematocysts of the ephyra stages of *Aurelia*, *Chrysaora*, *Cyanea*, and *Rhopilema* (Cnidaria, Scyphozoa). *Trans. Am. Microsc. Soc.* 96, 13–19. doi: 10.2307/3225958
- Calder, D. R. (1983). Nematocysts of stages in the life cycle of *Stomolophus meleagris*, with keys to scyphistomae and ephyrae of some western Atlantic Scyphozoa. *Can. J. Zool.* 61, 1185–1192. doi: 10.1139/z83-161
- Canepa, A., Fuentes, V., Sabatés, A., Piraino, S., Boero, F., and Gili, J. M. (2014). "Pelagia noctiluca in the Mediterranean Sea," in *Jellyfish Blooms*, eds K. A. Pitt and C. H. Lucas (Dordrecht: Springer), 237–266. doi: 10.1007/978-94-007-7015-7_11
- Cegolon, L., Heymann, W. C., Lange, J. H., and Mastrangelo, G. (2013). Jellyfish stings and their management: a review. *Mar. Drugs* 11, 523–550. doi: 10.3390/md11020523
- Ceh, J., Gonzalez, J., Pacheco, A. S., and Riascos, J. M. (2015). The elusive life cycle of scyphozoan jellyfish-metagenesis revisited. *Sci. Rep.* 5:12037. doi: 10.1038/srep12037
- De Donno, A., Idolo, A., Bagordo, F., Grassi, T., Leomanni, A., Serio, F., et al. (2014). Impact of stinging jellyfish proliferations along south Italian coasts: human health hazards, treatment and social costs. *Int. J. Environ. Res. Public Health* 11, 2488–2503. doi: 10.3390/ijerph110302488
- Di Camillo, C., Bo, M., Puce, S., Tazioli, S., and Bavestrello, G. (2006). The cnidome of *Carybdea marsupialis* (Cnidaria: Cubomedusae) from the Adriatic Sea. *J. Mar. Biol. Assoc. U. K.* 86, 705–709. doi: 10.1017/S0025315406013609
- Doyle, T. K., Headlam, J. L., Wilcox, C. L., MacLoughlin, E., and Yanagihara, A. A. (2017). Evaluation of *Cyanea capillata* sting management protocols using *ex vivo* and *in vitro* envenomation models. *Toxins* 9:215. doi: 10.3390/toxins9070215
- Fautin, D. G. (2009). Structural diversity, systematics, and evolution of cnidae. *Toxicon* 54, 1054–1064. doi: 10.1016/j.toxicon.2009.02.024

- Fuentes, V., Straehler-Pohl, I., Atienza, D., Franco, I., Tilves, U., Gentile, M., et al. (2011). Life cycle of the jellyfish *Rhizostoma pulmo* (Scyphozoa: Rhizostomeae) and its distribution, seasonality and inter-annual variability along the Catalan Coast and the Mar Menor (Spain, NW Mediterranean). *Mar. Biol.* 158, 2247–2266. doi: 10.1007/s00227-011-1730-7
- Gili, J. M., and Pagès, F. (2005). Jellyfish blooms. *Boll. Soc. Hist. Nat. Balears* 48, 9–22.
- Hall, A. H. (2018). I *Pelagia noctiluca* Jellyfish: can lesions and symptoms be prevented or ameliorated? *J. Mar. Biol. Aquac.* 4, 48–52.
- Heins, A., Glatzel, T., and Holst, S. (2015). Revised descriptions of the nematocysts and the asexual reproduction modes of the scyphozoan jellyfish *Cassiopea andromeda* (Forskål, 1775). *Zoomorphology* 134, 351–366. doi: 10.1007/s00435-015-0263-x
- Helm, R. R. (2018). Evolution and development of scyphozoan jellyfish. *Biol. Rev.* 93, 1228–1250. doi: 10.1111/brv.12393
- Helm, R. R., Tiozzo, S., Lilley, M. K., Lombard, F., and Dunn, C. W. (2015). Comparative muscle development of scyphozoan jellyfish with simple and complex life cycles. *EvoDevo* 6:11.
- Holst, S. (2012). Morphology and development of benthic and pelagic life stages of North Sea jellyfish (Scyphozoa, Cnidaria) with special emphasis on the identification of ephyra stages. *Mar. Biol.* 159, 2707–2722. doi: 10.1007/s00227-012-2028-0
- Holst, S., Sötje, I., Tiemann, H., and Jarms, G. (2007). Life cycle of the rhizostome jellyfish *Rhizostoma octopus* (L.) (Scyphozoa, Rhizostomeae), with studies on cnidocysts and statoliths. *Mar. Biol.* 151, 1695–1710. doi: 10.1007/s00227-006-0594-8
- Jarms, G. (2010). The early life history of Scyphozoa with emphasis on Coronatae a review with a list of described life cycles. *Verh. Naturwiss. Ver. Hambg.* 45, 17–31.
- Jarms, G., Tiemann, H., and Bämstedt, U. (2002). Development and biology of *Periphylla periphylla* (Scyphozoa: Coronatae) in a Norwegian fjord. *Mar. Biol.* 141, 647–657. doi: 10.1007/s00227-002-0858-x
- Kienberger, K., Riera-Buch, M., Schönemann, A. M., Bartsch, V., Halbauer, R., and Prieto, L. (2018). First description of the life cycle of the jellyfish *Rhizostoma luteum* (Scyphozoa: Rhizostomeae). *PLoS One* 13:e0202093. doi: 10.1371/journal.pone.0202093
- Kikinger, R. (1992). *Cotylorhiza tuberculata* (Cnidaria: Scyphozoa). Life history of a stationary population. *Mar. Ecol.* 13, 333–362. doi: 10.1111/j.1439-0485.1992.tb00359.x
- Kikinger, R., and von Salvini-Plawen, L. (1995). Development from polyp to stauromedusa in Stylocoronella (Cnidaria: Scyphozoa). *J. Mar. Biol. Assoc. U. K.* 7, 899–912. doi: 10.1017/S0025315400038236
- Killi, N., Bonello, G., Mariottini, G. L., Pardini, P., Pozzolini, M., and Cengiz, S. (2020). Nematocyst types and venom effects of *Aurelia aurita* and *Velella velella* from the Mediterranean Sea. *Toxicon* 175, 57–63. doi: 10.1016/j.toxicon.2019.12.155
- Kingsford, M. J., Becken, S., Bordehore, C., Fuentes, V. L., Pitt, K. A., and Yanagihara, A. A. (2018). Empowering stakeholders to manage stinging jellyfish: a perspective. *Coast. Manag.* 46, 1–18. doi: 10.1080/08920753.2018.1405326
- Kitatani, R., Yamada, M., Kamio, M., and Nagai, H. (2015). Length is associated with pain: jellyfish with painful sting have longer nematocyst tubules than harmless jellyfish. *PLoS One* 10:e0135015. doi: 10.1371/journal.pone.0135015
- Krasinska, S. (1914). Beitrage zur histologie der medusen. *Zwiss. Zool.* 109, 256–348.
- Larson, R. J. (1987). A note on the feeding, growth, and reproduction of the epipelagic scyphomedusa *Pelagia noctiluca* (Forskål). *Biol. Oceanogr.* 4, 447–454. doi: 10.1080/01965581.1987.10749501
- Lotan, A., Ben-Hillel, R., and Loya, Y. (1992). Life cycle of *Rhopilema nomadica*: a new immigrant scyphomedusan in the Mediterranean. *Mar. Biol.* 112, 237–242. doi: 10.1007/BF00702467
- Marambio, M., Ballesteros, A., López, L., Fuentes, V. L., and Gili, J. M. (2021a). *Guía de Identificación de Medusas y Otros Organismos Gelatinosos*. Available online at: <http://hdl.handle.net/10261/245294> (accessed July 6, 2021)
- Marambio, M., Canepa, A., Loópez, L., Gauci, A. A., Gueroun, S. K. M., Zampardi, S., et al. (2021b). Unfolding jellyfish bloom dynamics along the mediterranean basin by transnational citizen science initiatives. *Diversity* 13:274. doi: 10.3390/d13060274
- Marchini, B., De Nuccio, L., Mazzei, M., and Mariottini, G. L. (2004). A fast centrifuge method for nematocyst isolation from *Pelagia noctiluca* Forskal (Cnidaria: Scyphozoa). *Riv. Biol.* 97, 505–515.
- Mariottini, G. L., Giacco, E., and Pane, L. (2008). The mauve stinger *Pelagia noctiluca* (Forskål, 1775). Distribution, ecology, toxicity and epidemiology of stings. A review. *Mar. Drugs* 6, 496–513. doi: 10.3390/md20080025
- Mariscal, R. N. (1974). “Nematocysts,” in *Coelenterate Biology*, eds L. Muscatine and H. M. Lenhoff (New York, NY: Academic Press), 129–178.
- Martin, V. J., and Chia, F. S. (1982). Fine structure of a scyphozoan planula, *Cassiopeia xamachana*. *Biol. Bull.* 163, 320–328. doi: 10.2307/1541269
- Matveev, I. V., Adonin, L. S., Shaposhnikova, T. G., and Podgornaya, O. I. (2012). *Aurelia aurita*-cnidarian with a prominent medusoid stage. *J. Exp. Zool. B Mol. Dev. Evol.* 318, 1–12. doi: 10.1002/jez.b.21440
- Milisenda, G., Rossi, S., Vizzini, S., Fuentes, V., Purcell, J. E., Tilves, U., et al. (2018). Seasonal variability of diet and trophic level of the gelatinous predator *Pelagia noctiluca* (Scyphozoa). *Sci. Rep.* 8:12140.
- Montgomery, L., Seys, J., and Mees, J. (2016). To pee, or not to pee: a review on envenomation and treatment in European jellyfish species. *Mar. Drugs* 14:127. doi: 10.3390/md14070127
- Morabito, R., Cornara, L., La Spada, G., Marino, A., Mariottini, G. L., Remigante, A., et al. (2020). Inhibitory effect of plant extracts on the cytotoxicity of eurytele nematocysts from *Pelagia noctiluca*. *J. Biol. Res. Boll. Soc. Ital. Biol. Sper.* 93, 96–101. doi: 10.4081/jbr.2020.9136
- Morabito, R., Marino, A., Dossena, S., and La Spada, G. (2014). Nematocyst discharge in *Pelagia noctiluca* (Cnidaria, Scyphozoa) oral arms can be affected by lidocaine, ethanol, ammonia and acetic acid. *Toxicon* 83, 52–58. doi: 10.1016/j.toxicon.2014.03.002
- Morandini, A. C., Da Silveira, F. L., and Jarms, G. (2004). The life cycle of *Chrysaora lactea* Eschscholtz, 1829 (Cnidaria, Scyphozoa) with notes on the scyphistoma stage of three other species. *Hydrobiologia* 530, 347–354. doi: 10.1007/978-1-4020-2762-8_40
- Morandini, A. C., and Marques, A. C. (2010). Revision of the genus *Chrysaora* Péron & Lesueur, 1810 (Cnidaria: Scyphozoa). *Zootaxa* 2464, 1–97. doi: 10.11646/zootaxa.2464.1.1
- Morandini, A. C., Silveira, F. D., and Cornelius, P. F. (2006). Redescription of *Chrysaora lactea* Eschscholtz, 1829 (Cnidaria, Scyphozoa) from the Brazilian coast, with designation of a neotype. *Zootaxa* 1135, 29–48. doi: 10.5281/zenodo.171956
- Östman, C. (1989). “Nematocysts as taxonomic criteria within the family Campanulariidae, Hydrozoa,” in *The Biology of Nematocysts*, eds D. A. Hessinger and H. M. Lenhoff (San Diego, CA: Academic Press), 501–517. doi: 10.1016/b978-0-12-345320-4.50031-6
- Östman, C. (1991). “Scanning electron microscopic observations on Scandinavian scyphozoans with special reference to their nematocysts”, in *Proceedings of the 2nd Workshop on Jellyfish in the Mediterranean Sea*. Map Technical Rep Ser. 47 (Athens: UNEP), 283–292.
- Östman, C. (2000). A guideline to nematocyst nomenclature and classification, and some notes on the systematic value of nematocysts. *Sci. Mar.* 64, 31–46. doi: 10.3989/scimar.2000.64s131
- Östman, C., and Hydman, J. (1997). Nematocyst analysis of *Cyanea capillata* and *Cyanea lamarkii* (Scyphozoa, Cnidaria). *Sci. Mar.* 61, 313–344.
- Östman, C., Kultima, J. R., Roat, C., and Rundblom, K. (2010a). Acontia and mesentery nematocysts of the sea anemone *Metridium senile* (Linnaeus, 1761) (Cnidaria: Anthozoa). *Sci. Mar.* 74, 483–497. doi: 10.3989/scimar.2010.74n3483
- Östman, C., Kultima, J. R., and Wong, S. Y. G. (2010b). Dart formation in nematocysts of the sea anemone *Metridium senile* (Linnaeus, 1761) (Cnidaria: Anthozoa). *Sci. Mar.* 74, 499–510. doi: 10.3989/scimar.2010.74n3499
- Piraino, S., Aglieri, G., Martell, L., Mazzoldi, C., Melli, V., Milisenda, G., et al. (2014). *Pelagia benovici* sp. nov. (Cnidaria, Scyphozoa): a new jellyfish in the Mediterranean Sea. *Zootaxa* 3794, 455–468. doi: 10.11646/zootaxa.3794.3.7
- Purcell, J. E. (1984). The functions of nematocysts in prey capture by epipelagic siphonophores (Coelenterata, Hydrozoa). *Biol. Bull.* 166, 310–327. doi: 10.2307/1541219
- Purcell, J. E., and Mills, C. E. (1988). “The correlation of nematocyst types to diets in pelagic Hydrozoa,” in *The Biology of Nematocysts*, eds D. A. Hessinger and H. M. Lenhoff (New York, NY: Academic Press), 463–485. doi: 10.1016/b978-0-12-345320-4.50029-8

- Purcell, J. E., Uye, S., and Lo, W. (2007). Anthropogenic causes of jellyfish blooms and their direct consequences for humans: a review. *Mar. Ecol. Prog. Ser.* 350, 153–174. doi: 10.3354/meps07093
- Quadrifoglio, F., Avian, M., Del Negro, P., Princi, T., Scuka, M., Gavinelli, E., et al. (1986). Nematocisti e tossine di *Pelagia noctiluca*. *Nova Thalassia* 8, 155–162.
- R Core Team (2017). *A Language and Environment for Statistical Computing*. Vienna: R Foundation for Statistical Computing.
- Ramondenc, S., Ferrieux, M., Collet, S., Benedetti, F., Guidi, L., and Lombard, F. (2019). From egg to maturity: a closed system for complete life cycle studies of the holopelagic jellyfish *Pelagia noctiluca*. *J. Plankton Res.* 41, 207–217. doi: 10.1093/plankt/fbz013
- Richardson, A. J., Bakun, A., Hays, G. C., and Gibbons, M. J. (2009). The jellyfish joyride: causes, consequences and management responses to a more gelatinous future. *Trends ecol. Evol.* 24, 312–322. doi: 10.1016/j.tree.2009.01.010
- Rottini Sandrini, L., and Avian, M. (1983). Biological cycle of *Pelagia noctiluca*: morphological aspects of the development from planula to ephyra. *Mar. Biol.* 74, 169–174. doi: 10.1007/BF00413920
- Russell, F. S. (1970). *The medusae of the British Isles II. Pelagic Siphonophora with a Supplement to the First Volume on Hydromedusae*. Cambridge: Cambridge University Press.
- Sabatés, A., Pages, F., Atienza, D., Fuentes, V., Purcell, J. E., and Gili, J.-M. (2010). “Planktonic cnidarian distribution and feeding of *Pelagia noctiluca* in the NW Mediterranean Sea,” in *Jellyfish Blooms: New Problems and Solutions*, eds J. E. Purcell and D. L. Angel (Dordrecht: Springer), 153–165. doi: 10.1007/s10750-010-0221-z
- Sánchez-Rodríguez, J., and Lucio-Martínez, N. L. (2011). Isolation and prepurification of active compounds in venom from *Pelagia noctiluca* (Scyphozoa: Pelagiidae) from the Caribbean Sea. *Cienc. Mar.* 37, 369–377. doi: 10.7773/cm.v37i3.1893
- Schiariti, A., Kawahara, M., Uye, S., and Mianzan, H. W. (2008). Life cycle of the jellyfish *Lychnorhiza lucerna* (Scyphozoa: Rhizostomeae). *Mar. Biol.* 156, 1–12. doi: 10.1007/s00227-008-1050-8
- Shostak, S., and Kolluri, V. (1995). Symbiogenetic origins of cnidarian cnidocysts. *Symbiosis* 19, 1–29.
- Straehler-Pohl, I., and Jarms, G. (2010). Identification key for young ephyrae: a first step for early detection of jellyfish blooms. *Hydrobiologia* 645, 3–21. doi: 10.1007/978-90-481-9541-1_2
- Straehler-Pohl, I., Widmer, C. L., and Morandini, A. C. (2011). Characterizations of juvenile stages of some semeanostome Scyphozoa (Cnidaria), with recognition of a new family (Phacellophoridae). *Zootaxa* 2741, 1–37. doi: 10.11646/zootaxa.2741.1.1
- Strömberg, S. M., and Östman, C. (2017). The cnidome and internal morphology of *Lophelia pertusa* (Linnaeus, 1758) (Cnidaria, Anthozoa). *Acta Zool.* 98, 191–213. doi: 10.1111/azo.12164
- Strömberg, S. M., Östman, C., and Larsson, A. I. (2019). The cnidome and ultrastructural morphology of late planulae in *Lophelia pertusa* (Linnaeus, 1758) with implications for settling competency. *Acta Zool.* 100, 431–450. doi: 10.1111/azo.12296
- Tilves, U., Purcell, J. E., Fuentes, V. L., Torrents, A., Pascual, M., Raya, V., et al. (2016). Natural diet and predation impacts of *Pelagia noctiluca* on fish eggs and larvae in the NW Mediterranean. *J. Plankton Res.* 38, 1243–1254. doi: 10.1093/plankt/fbw059
- Uchida, T. (1934). Metamorphosis of a Scyphomedusa (*Pelagia panopyra*). *Proc. Imp. Acad.* 10, 428–430. doi: 10.2183/pjab1912.10.428
- Watson, G. M., and Wood, R. L. (1988). “Colloquium on terminology,” in *The Biology of Nematocysts*, eds D. A. Hessinger and H. M. Lenhoff (San Diego, CA: Academic Press), 21–23. doi: 10.1016/b978-0-12-345320-4.50006-7
- Weill, R. (1934). “Contribution à l’ étude des cnidaires et de leurs nématocystes. I, II,” in *Travaux de la Station Zoologique de Wimereux, 10 and 11* (Paris: Laboratoire d’évolution des êtres organisés), 1–701.
- Widmer, C. L. (2008). Life cycle of *Chrysaora fuscescens* (Cnidaria: Scyphozoa) and a Key to sympatric ephyrae. *Pac. Sci.* 62, 71–82. doi: 10.2984/1534-6188(2008)62[71:lcofc]2.0.co;2
- WoRMS (World Register of Marine Species) (2020). Available online at: <http://www.marinespecies.org/aphia.php?p=taxdetails&tid=851656> (accessed July 20, 2020)
- Yuan, D., Nakanishi, N., Jacobs, D., and Hartenstein, V. (2008). Embryonic development and metamorphosis of the scyphozoan *Aurelia*. *Dev. Genes Evol.* 218, 525–539. doi: 10.1007/s00427-008-0254-8
- Yue, Y., Xue, W., Yu, H., Li, R., and Li, P. (2020). Updated descriptions of the nematocysts of the scyphozoan jellyfish *Cyanea nozakii* Kishinouye, 1891 (Cnidaria, Scyphozoa). *Toxicon* 187, 271–278. doi: 10.1016/j.toxicon.2020.09.016

Conflict of Interest: MN was employed by ISDIN company.

The remaining authors declare that the research was conducted in the absence of any commercial or financial relationships that could be construed as a potential conflict of interest.

Publisher’s Note: All claims expressed in this article are solely those of the authors and do not necessarily represent those of their affiliated organizations, or those of the publisher, the editors and the reviewers. Any product that may be evaluated in this article, or claim that may be made by its manufacturer, is not guaranteed or endorsed by the publisher.

Copyright © 2021 Ballesteros, Östman, Santín, Marambio, Narda and Gili. This is an open-access article distributed under the terms of the Creative Commons Attribution License (CC BY). The use, distribution or reproduction in other forums is permitted, provided the original author(s) and the copyright owner(s) are credited and that the original publication in this journal is cited, in accordance with accepted academic practice. No use, distribution or reproduction is permitted which does not comply with these terms.